

Fermionic versus bosonic thermalization in phonon-driven exciton dynamics: An analytic dimensionality study

Manuel Katzer ^{*}, Malte Selig, and Andreas Knorr

*Technische Universität Berlin, Institut für Theoretische Physik, Nichtlineare Optik und Quantenelektronik,
Hardenbergstraße 36, 10623 Berlin, Germany*

 (Received 4 October 2023; revised 9 February 2024; accepted 6 March 2024; published 2 April 2024)

Excitons are compound particles formed from an electron and a hole in semiconductors. The impact of this substructure on the phonon-exciton interaction is described by a closed system of microscopic scattering equations. To calculate the actual excitonic thermalization properties beyond the pure bosonic picture, this equation is derived directly from an electron-hole picture within the Heisenberg equation of motion framework. In addition to the well-known bosonic character of the compound particles, we identified processes of a repulsive, fermionic type, as well as attractive carrier exchange contributing to the scattering process. In this analytical study we give general statements about the thermalization of excitons in two- and three-dimensional semiconductors. We give insights on the strong dependence of the thermalization characteristics of the exciton Bohr radius and the thermalization wavelength. Above all, we analytically provide arguments why a bosonic behavior of excitons—such as an enhanced ground-state occupation—requires the dominant phonon scattering to be quasielastic. Acoustic phonons tend to fulfill this, as each scattering event only takes small amounts of energy out of the distribution, while optical phonons tend to prevent macroscopic occupations of the lowest exciton state, since the Pauli repulsion between the individual carriers will then dominate the thermalization dynamics.

DOI: [10.1103/PhysRevB.109.155110](https://doi.org/10.1103/PhysRevB.109.155110)

I. INTRODUCTION

van der Waals heterostructures of atomically thin semiconductors sparked new hope to find bosonic or even macroscopic occupation effects of excitons, since they can host long-living excitonic interlayer states [1–7]. The discussion whether semiconductor excitons can show macroscopic occupation and spontaneous emergence of coherence dates back more than half a century [8–11], and there are reports of experimental signatures of related effects also for excitons in other semiconductor platforms, e.g., in GaAs quantum wells [12,13], in quantum hall systems [14], and recently in bulk Cu₂O [15].

The last decades have also seen quite a few theoretical approaches towards effects of macroscopic occupation and spontaneous coherence in excitonic systems, and even more on exciton-polaritons. There is, e.g., the quantum kinetic approach from the Haug group [16–19] and also an abundance of other theory works, e.g., Refs. [20–31]. They are very diverse in their theoretical approaches, however, to our understanding, they all implicitly or explicitly share one key assumption, namely, that excitons are pure bosons also for densities beyond the classical Maxwell-Boltzmann limit, which is a necessary condition to apply Bogoliubov approximations or Gross-Pitaevskii approaches [32]. It was, however, also shown in several works that the fermionic substructure of excitons cannot be neglected at elevated densities [33–38]. In a recent numerical study [39], we challenged the assumption of pure bosonic thermalization, presenting an excitonic Boltzmann

scattering equation to account for phonon-mediated excitonic thermalization above the classical Maxwell-Boltzmann limit, taking the fermionic substructure into account. We showed that for large parts of the parameter space, fermionic Pauli blocking inhibits bosonic thermalization, thus resulting in effects such as macroscopic ground-state occupations. The equations of motion we study here, as derived and numerically approached in Ref. [39], are, in principle, valid for Wannier-type excitons of arbitrary dimension in semiconductors. However, they do not apply for Frenkel-type excitons, as they are, for instance, described in organic semiconductors or molecular aggregates [40–42].

In the present study we provide analytic limits of a generalized exciton-phonon interaction dynamics, allowing us to deduce statements on the nature of the exciton as a particle between boson and fermion in a more general framework and predict its behavior in two and three dimensions and in a unitless and therefore material insensitive description. We show that three parameters influence the thermalization, namely, the exciton Bohr radius a_0 , the thermal de Broglie wavelength λ_{th} , and their value relative to the phonon momentum Q_{phon} , which couples to the excitonic ground mode $\mathbf{Q} = 0$. The two main findings are as follows: The Bohr radius of the exciton needs to be significantly smaller than the thermal wavelength, and only when the dominant exciton-phonon scattering process is elastic enough, stimulated scattering to the ground state can win over the Pauli repulsion between the carriers which constitute the excitons, as inelastic optical phonon scattering favors Pauli blocking over stimulated scattering. The results from our analytic computations presented in this work are in

^{*}manuel.katzer@physik.tu-berlin.de

good agreement with the numerically obtained findings we presented in Ref. [39], and thus offer a deeper understanding of these results.

The paper is structured as follows: In Sec. II we present the excitonic Boltzmann equation which was derived in Ref. [39], and the individual contributions within the equation are recapitulated. In Sec. III we give a detailed discussion on the analytic limit of low temperatures and derive analytic expressions allowing interpretation of the behavior of excitons at low temperatures at the threshold of the first deviation from the classical Maxwell-Boltzmann limit. In Sec. IV we give visualizations of the analytic expressions and discuss the resulting requirements for bosonic or fermionic thermalization behavior of excitons in two or three dimensions. In Sec. V we conclude.

II. EXCITONIC BOLTZMANN EQUATION

This section is a brief recapitulation of the equation that was derived and introduced in Ref. [39], before we examine its analytical limits in detail in the subsequent sections. The kinetic equation describes the dynamics of the exciton occupation,

$$N_{\mathbf{Q}}^{\nu} = \sum_{\mathbf{q}\mathbf{q}'} (\varphi_{\mathbf{q}}^{\nu})^* \varphi_{\mathbf{q}'}^{\nu} \langle v_{\mathbf{q}+\tilde{\alpha}\mathbf{Q}}^{\dagger} c_{\mathbf{q}-\tilde{\beta}\mathbf{Q}}^{\dagger} c_{\mathbf{q}'-\tilde{\beta}\mathbf{Q}}^{\dagger} v_{\mathbf{q}'+\tilde{\alpha}\mathbf{Q}} \rangle^c, \quad (1)$$

with center-of-mass momentum \mathbf{Q} and the excitonic Rydberg state ν , where $\varphi_{\mathbf{q}}^{\nu}$ accounts for the real-space relative motion wave function of the exciton gained from solving the Wannier equation [43]. The wave functions represent a full orthonormalized set $\sum_{\mathbf{q}} (\varphi_{\mathbf{q}}^{\lambda})^* \varphi_{\mathbf{q}}^{\nu} = \delta^{\lambda\nu}$, while $c_{\mathbf{q}}^{(\dagger)}$ and $v_{\mathbf{q}}^{(\dagger)}$ are the fermionic annihilation (creation) operators for carriers in the conduction band and the valence band, respectively. The relative electron and hole masses $\tilde{\alpha} = \frac{m_e}{M}$ and $\tilde{\beta} = \frac{m_h}{M}$ abbreviate the respective proportion of the exciton mass $M = m_e + m_h$.

It is important to state that for the derivation of the equation of motion for $N_{\mathbf{Q}}^{\nu}$ in Ref. [39] we started from the fundamental electronic semiconductor Hamiltonian [44], which allowed us to account for bosonic and fermionic properties of the exciton thermalization:

$$\begin{aligned} H = & \sum_{\mathbf{k}\lambda} \epsilon_{\mathbf{k}}^{\lambda} \lambda_{\mathbf{k}}^{\dagger} \lambda_{\mathbf{k}} + \sum_{\mathbf{q}\alpha} \hbar \omega_{\mathbf{q}}^{\alpha} b_{\mathbf{q}}^{\dagger \alpha} b_{\mathbf{q}}^{\alpha} \\ & + \frac{1}{2} \sum_{\lambda\lambda' \mathbf{k}\mathbf{k}'\mathbf{q}} V_{\mathbf{q}} \lambda_{\mathbf{k}}^{\dagger} \lambda_{\mathbf{k}'}^{\dagger} \lambda_{\mathbf{k}'+\mathbf{q}} \lambda_{\mathbf{k}-\mathbf{q}} \\ & + \sum_{\mathbf{k}\mathbf{q}\lambda\alpha} g_{\mathbf{q}}^{\lambda\alpha} \lambda_{\mathbf{k}+\mathbf{q}}^{\dagger} \lambda_{\mathbf{k}} (b_{\mathbf{q}}^{\alpha} + b_{-\mathbf{q}}^{\dagger \alpha}). \end{aligned} \quad (2)$$

The first term accounts for the dispersion of electrons, parametrized from density-functional theory (DFT) calculations in the effective mass approximation [45]. In the conduction band, the band index is $\lambda = c$, and in the valence band $\lambda = v$, while \mathbf{k} refers to the momentum \mathbf{k} , respectively. The second term accounts for the dispersion of phonons. The mode index α accounts for acoustic and optical phonon modes, parametrized by *ab initio* values from the literature, for transition metal dichalcogenide (TMDC) excitons; see, e.g., Refs. [46–48]. The third term accounts for the Coulomb interaction between electrons and holes. The coupling element $V_{\mathbf{q}}$ is obtained from an analytic solution

of the Poisson equation for the Rytova-Keldysh potential [49,50]. The fourth term accounts for the electron-phonon interaction in the valence and conduction band. The appearing electron-phonon coupling elements $g_{\mathbf{q}}^{\lambda\alpha}$, for the different involved phonon modes α in the two bands $\lambda = c, v$, are treated in the effective deformation potential approximation, parametrized with values typically obtained from DFT calculations; see, e.g., for TMDCs Refs. [47,48,51–53].

The excitonic Boltzmann scattering equation in the Born-Markov limit was derived in Ref. [39] from the fundamental electronic semiconductor Hamiltonian, Eq. (2). It is valid for a not-too-strong exciton-phonon coupling, which does not induce a fast time dependence of the exciton distribution function on the timescale of the phonon oscillation frequency. This is common for many semiconductor materials [17,51,54–57], as long as the initial pulsed excitation does not break this limit. This allows treating the appearing hierarchy problem in the second-order Born-Markov approximation [55]. In situations where this approximation does not hold, higher-order perturbation or a nonperturbative calculation would have to be taken into account by, for instance, including higher orders in the Born approximation [58,59], applying quantum kinetic approaches [18,60], by utilizing a polaron framework [61–63], or employing path integral methods [63,64]. Further studies on the relevance of non-Markovian effects can be found, e.g., in Refs. [58,65,66]. Compared to a classical Boltzmann equation, this novel equation comprises terms second order in $N_{\mathbf{Q}}^{\nu}$, which were obtained by applying the unit operator technique [33,35,36], allowing to project the fermionic expectation operators on excitonic pair occupation operators. The strict calculation in the electronic picture also circumvents difficulties in the factorization of excitonic expectation values. For details on the derivation, see Ref. [39] and Appendix A. The resulting equation reads

$$\partial_t N_{\mathbf{Q}}^{\nu} = \partial_t N_{\mathbf{Q}}^{\nu}|_{\text{class}} + \partial_t N_{\mathbf{Q}}^{\nu}|_{\text{bos}} + \partial_t N_{\mathbf{Q}}^{\nu}|_{\text{ferm}} + \partial_t N_{\mathbf{Q}}^{\nu}|_{\text{exc}}. \quad (3)$$

The first term in Eq. (3) accounts for the linear contribution, responsible for a thermalization according to the classical Maxwell-Boltzmann statistics. It is valid for dilute, classical exciton gases [53,67,68] and reads

$$\partial_t N_{\mathbf{Q}}^{\nu}|_{\text{class}} = \frac{2\pi}{\hbar} \sum_{\mathbf{Q}'\lambda} (W_{\mathbf{Q}\mathbf{Q}'}^{\lambda\nu} N_{\mathbf{Q}'}^{\lambda} - W_{\mathbf{Q}\mathbf{Q}'}^{\nu\lambda} N_{\mathbf{Q}}^{\nu}), \quad (4)$$

with the scattering tensor

$$\begin{aligned} W_{\mathbf{Q}\mathbf{Q}'}^{\nu\lambda} = & \sum_{\alpha} |g_{|\mathbf{Q}-\mathbf{Q}'|,\alpha}^{\nu\lambda}|^2 ((1 + n_{|\mathbf{Q}-\mathbf{Q}'|}^{\alpha}) \delta(\mathcal{E}_{\mathbf{Q}'}^{\lambda} - \mathcal{E}_{\mathbf{Q}}^{\nu} + \hbar\omega_{|\mathbf{Q}-\mathbf{Q}'|}^{\alpha}) \\ & + n_{|\mathbf{Q}-\mathbf{Q}'|}^{\alpha} \delta(\mathcal{E}_{\mathbf{Q}'}^{\lambda} - \mathcal{E}_{\mathbf{Q}}^{\nu} - \hbar\omega_{|\mathbf{Q}-\mathbf{Q}'|}^{\alpha})). \end{aligned} \quad (5)$$

The exciton-phonon coupling reads

$$g_{\mathbf{Q},\alpha}^{\nu\nu'} = \sum_{\mathbf{q}} (g_{\mathbf{Q}}^{c\alpha} (\varphi_{\mathbf{q}}^{\nu})^* \varphi_{\mathbf{q}-\tilde{\beta}\mathbf{Q}}^{\nu'} - g_{\mathbf{Q}}^{v\alpha} (\varphi_{\mathbf{q}}^{\nu})^* \varphi_{\mathbf{q}+\tilde{\alpha}\mathbf{Q}}^{\nu'}) \quad (6)$$

and depends on convolutions of exciton wave functions $\varphi_{\mathbf{q}}^{\nu}$ and the electron-phonon coupling element $g_{\mathbf{q}}^{\lambda\alpha}$ from the electronic Hamiltonian, Eq. (2).

For densities above the classical limit, additionally three nonlinearities become important, all in the same order of the

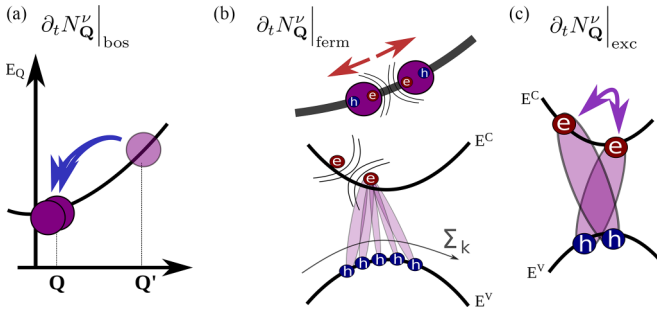


FIG. 1. Recapitulation of the different nonlinear effects in the excitonic thermalization process, as introduced in detail in Ref. [39]. (a) The nonlinearity $\partial_t N_{\mathbf{Q}}^{\nu}|_{\text{bos}}$ leads to stimulated scattering, similar to pure bosonic particles. (b) The fermionic correction term $\partial_t N_{\mathbf{Q}}^{\nu}|_{\text{ferm}}$ leads to a repulsion as electrons (and holes) show Pauli blocking. Many excitons contribute to this effect at a given momentum, illustrated by the summation over k in the lower panel. (c) The exchange nonlinearity, $\partial_t N_{\mathbf{Q}}^{\nu}|_{\text{exc}}$, is of attractive nature. It is due to a carrier exchange during the scattering process. Figure adapted from [39].

exciton density

$$\bar{n} = \frac{1}{L^d} \sum_{\mathbf{Q}^{\nu}} N_{\mathbf{Q}^{\nu}}^{\nu}, \quad (7)$$

with a factor L^d of unit $[L^d] = \text{nm}^d$, i.e., an area or a volume, dependent on the dimension $d \in \{2, 3\}$, which we introduce here as an index to allow for a more general formulation throughout the whole manuscript. The nonlinearities are all sketched in Fig. 1. The second term in Eq. (3) accounts for bosonic stimulated scattering, which would also occur for pure bosons [17], see Fig. 1(a):

$$\partial_t N_{\mathbf{Q}}^{\nu}|_{\text{bos}} = \frac{2\pi}{\hbar} \sum_{\mathbf{Q}^{\lambda}} \Gamma_{\mathbf{Q}\mathbf{Q}^{\lambda}}^{B,\nu\lambda} N_{\mathbf{Q}^{\lambda}}^{\lambda} N_{\mathbf{Q}}^{\nu}. \quad (8)$$

The respective scattering matrix can be directly computed from the classical scattering matrix $W_{\mathbf{Q}\mathbf{Q}^{\lambda}}^{\nu\lambda}$, Eq. (5), and reads

$$\begin{aligned} \Gamma_{\mathbf{Q}\mathbf{Q}^{\lambda}}^{B,\nu\lambda} &= W_{\mathbf{Q}\mathbf{Q}^{\lambda}}^{\nu\lambda} - W_{\mathbf{Q}\mathbf{Q}}^{\lambda\nu} \\ &= \sum_{\alpha} |g_{\mathbf{Q}-\mathbf{Q}^{\lambda},\alpha}^{\nu\lambda}|^2 (\delta(\mathcal{E}_{\mathbf{Q}}^{\lambda} - \mathcal{E}_{\mathbf{Q}}^{\nu} - \hbar\omega_{\mathbf{Q}-\mathbf{Q}^{\lambda}}^{\alpha}) \\ &\quad - \delta(\mathcal{E}_{\mathbf{Q}}^{\lambda} - \mathcal{E}_{\mathbf{Q}}^{\nu} + \hbar\omega_{\mathbf{Q}-\mathbf{Q}^{\lambda}}^{\alpha})). \end{aligned} \quad (9)$$

The mentioned stimulated scattering of this bosonic nonlinear contribution, Eq. (8), leads to amplified scattering to already strongly occupied states, and thus enables high occupations of the ground state at $\mathbf{Q} = 0$.

In addition to the classical and bosonic contributions to Eq. (3), two further nonlinearities occur due to the electronic substructure of the excitons. The third term in Eq. (3), see Fig. 1(b), is of repulsive nature and occurs due to Pauli blocking of the fermionic carriers the exciton is constituted of. It reads

$$\partial_t N_{\mathbf{Q}}^{\nu}|_{\text{ferm}} = \frac{2\pi}{\hbar} \sum_{\mathbf{Q}^{\lambda\nu'}} (\Gamma_{\mathbf{Q}\mathbf{Q}^{\lambda}}^{F,\nu\lambda,\nu'} N_{\mathbf{Q}}^{\lambda} - \Gamma_{\mathbf{Q}\mathbf{Q}^{\lambda}}^{F,\lambda\nu,\nu'} N_{\mathbf{Q}}^{\nu}) N_{\mathbf{Q}}^{\nu'}. \quad (10)$$

Note that compared to classical and bosonic contributions of Eq. (3), this repulsive term requires an additional convolution over all excitonic states, which originates from the projection into the excitonic basis. Similar to the scattering matrices above, we find here the three-dimensional scattering tensor

$$\begin{aligned} \Gamma_{\mathbf{Q}\mathbf{Q}^{\lambda}}^{F,\lambda\nu,\nu'} &= \sum_{\alpha} \text{Re}(g_{\mathbf{Q}-\mathbf{Q}^{\lambda},\alpha}^{\nu\lambda} g_{\mathbf{Q}\mathbf{Q}^{\lambda},\alpha}^{F,\lambda\nu,\nu'}) (\delta(\mathcal{E}_{\mathbf{Q}}^{\lambda} - \mathcal{E}_{\mathbf{Q}}^{\nu} - \hbar\omega_{\mathbf{Q}-\mathbf{Q}^{\lambda}}^{\alpha}) \\ &\quad - \delta(\mathcal{E}_{\mathbf{Q}}^{\lambda} - \mathcal{E}_{\mathbf{Q}}^{\nu} + \hbar\omega_{\mathbf{Q}-\mathbf{Q}^{\lambda}}^{\alpha})). \end{aligned} \quad (11)$$

Furthermore, there occurs a second nonlinearity due to the electronic substructure of the exciton, namely, the fourth term in Eq. (3), see Fig. 1(c). It results from exchanging carriers between excitons during the scattering and constitutes a typical fermionic exchange nonlinearity:

$$\partial_t N_{\mathbf{Q}}^{\nu}|_{\text{exc}} = \frac{2\pi}{\hbar} \sum_{\mathbf{K}\mathbf{K}'\lambda'\nu'} \Gamma_{\mathbf{Q}\mathbf{K}\mathbf{K}'}^{E,\nu\lambda'\nu'} N_{\mathbf{K}}^{\lambda'} N_{\mathbf{K}'}^{\nu'}. \quad (12)$$

Here, the respective scattering tensor reads

$$\begin{aligned} \Gamma_{\mathbf{Q}\mathbf{K}\mathbf{K}'}^{E,\nu\lambda'\nu'} &= \frac{1}{2} \sum_{\alpha\lambda} (g_{\mathbf{Q}-\mathbf{Q}^{\lambda},\alpha}^{\nu\lambda} g_{\mathbf{Q}\mathbf{K}\mathbf{K}'}^{E,\nu\lambda,\lambda',\nu'} + g_{\mathbf{Q}-\mathbf{Q}^{\lambda},\alpha}^{\lambda\nu} g_{\mathbf{Q}\mathbf{K}\mathbf{K}'}^{E,\lambda\nu,\lambda',\nu'}) \\ &\quad \times (\delta(\mathcal{E}_{\mathbf{Q}}^{\lambda} - \mathcal{E}_{\mathbf{Q}}^{\nu} - \hbar\omega_{\mathbf{Q}-\mathbf{Q}^{\lambda}}^{\alpha}) \\ &\quad - \delta(\mathcal{E}_{\mathbf{Q}}^{\lambda} - \mathcal{E}_{\mathbf{Q}}^{\nu} + \hbar\omega_{\mathbf{Q}-\mathbf{Q}^{\lambda}}^{\alpha})). \end{aligned} \quad (13)$$

For all contributions of Eq. (3), the coupling constants for the exciton-phonon coupling are given by the wave-function overlap of the involved carriers, which depend on the momenta \mathbf{Q}' of the phonons associated to the process. While for the classical a bosonic contribution, this is encoded in the well-known coupling $g_{\mathbf{Q}\mathbf{Q}^{\lambda},\alpha}^{\nu\lambda}$, Eq. (6), the new scattering tensors that arise due to the fermionic substructure come with new, more elaborate overlaps, namely, $g_{\mathbf{Q}\mathbf{Q}^{\lambda},\alpha}^{F,\lambda\nu,\nu'}$ for the fermionic nonlinearity, and $g_{\mathbf{Q}\mathbf{Q}^{\lambda},\alpha}^{E,\lambda\nu,\lambda',\nu'}$ for the exchange nonlinearity (see Appendix B for details). Their increased complexity reflects the convolution with all carriers involved, (i.e., also those of the other excitons). The fact that the fermionic scattering tensors depend on more overlapping excitonic wave functions compared to the classical and bosonic terms leads to a strong dependence of the relative dominance between the nonlinearities on the exciton Bohr radius a_0 . Large Bohr radii lead to smaller wave functions in momentum space. This will be crucial for the analytic discussion in the following section.

III. ANALYTICAL LIMIT

Equation (3) is a general result which is valid for excitons in different systems, thus also for systems with different dimensionality. The following discussion is thus conducted for two- and three-dimensional excitons, respectively, with TMDC excitons used to give an example of experimentally accessible parameter ranges in two dimensions. For our

analytical discussion, we rewrite Eq. (3) to a more compact form:

$$\begin{aligned} \partial_t N_{\mathbf{Q}}^{\nu} = & \frac{2\pi}{\hbar} \left[\sum_{\mathbf{Q}'\lambda} \left[(W_{\mathbf{Q}'\mathbf{Q}}^{\lambda\nu} (1 + N_{\mathbf{Q}}^{\nu}) - \sum_{\mathbf{K}\nu'} \Gamma_{\mathbf{Q}'\mathbf{Q},\mathbf{K}}^{F,\nu\lambda,\nu'} N_{\mathbf{K}}^{\nu'}) N_{\mathbf{Q}}^{\lambda} \right. \right. \\ & \left. \left. - (W_{\mathbf{Q}\mathbf{Q}'}^{\nu\lambda} (1 + N_{\mathbf{Q}'}^{\lambda}) - \sum_{\mathbf{K}\nu'} \Gamma_{\mathbf{Q}\mathbf{Q}',\mathbf{K}}^{F,\lambda\nu,\nu'} N_{\mathbf{K}}^{\nu'}) N_{\mathbf{Q}}^{\nu} \right] \right. \\ & \left. - \sum_{\mathbf{K}\mathbf{K}'\lambda'\nu'} \Gamma_{\mathbf{Q},\mathbf{K},\mathbf{K}'}^{E,\nu\lambda',\nu'} N_{\mathbf{K}}^{\lambda'} N_{\mathbf{K}'}^{\nu'} \right]. \end{aligned} \quad (14)$$

In order to identify parameter regimes where the thermalization is dominated by the bosonic nonlinearities, we introduce two general parameters, the Bohr radius a_0 and the thermal wavelength λ_{th} . To formally define an exciton Bohr radius, the $1s$ wave functions, which are accessed as the eigenfunctions of the Wannier equation, can be fitted to an analytical model [44], which in the two- and three-dimensional case read

$$\varphi_{\mathbf{q}}^{d=2} = \frac{8\sqrt{2\pi a_0^2/L^2}}{(4 + a_0^2 q^2)^{\frac{3}{2}}}, \quad \varphi_{\mathbf{q}}^{d=3} = \frac{8\sqrt{\pi a_0^3/L^3}}{(1 + a_0^2 q^2)^2}. \quad (15)$$

In the three-dimensional model, a_0 is directly equivalent to the extension of the exciton in real space, while for two dimensions, it is typically defined to be twice the radius of the extension [44]. TMDC excitons, for example, typically have extension radii in the order of 1 nm [69]; we therefore estimate the Bohr radius for TMDCs to be around 2 nm when we give examples in the following discussion. Furthermore, we introduce the thermal wavelength λ_{th} (also referred to as de Broglie wavelength), which depends on temperature T and effective exciton mass M :

$$\lambda_{th} = \frac{\hbar}{\sqrt{2Mk_B T}}. \quad (16)$$

The thermal wavelength λ_{th} characterizes a typical inverse wavelength extension of the occupation number distribution as a function of wave numbers in an ideal classical exciton gas at a specified temperature and thus is a well-defined parameter close to the classical limit [65]. In Sec. III B we will introduce an analytical expression for the exciton occupation in the classical limit, Eq. (21), from which we can read off that the inverse of λ_{th} marks the absolute value of the center-of-mass momentum $|\mathbf{Q}_{th}| = \frac{1}{\lambda_{th}}$, where, for this specific temperature and particle mass, the occupation (of a classical ensemble) is $N_{\mathbf{Q}_{th}} = \frac{1}{e} N_{\mathbf{Q}=0}$, and therefore λ_{th}^{-1} is directly linked to the mass- and temperature-dependent width of the occupation of a classical exciton occupation distribution in momentum space. This is typically used, e.g., to provide unitless plots of occupation distributions when discussing density-dependent phenomena which occur independent of temperature and particle mass; see, e.g., Bloch *et al.* [70]. In the following we discuss the analytical limits of Eq. (3).

A. Low-temperature limit

In the following analytic discussion of Eq. (3), we assume that the Bohr radius is small compared to the thermal

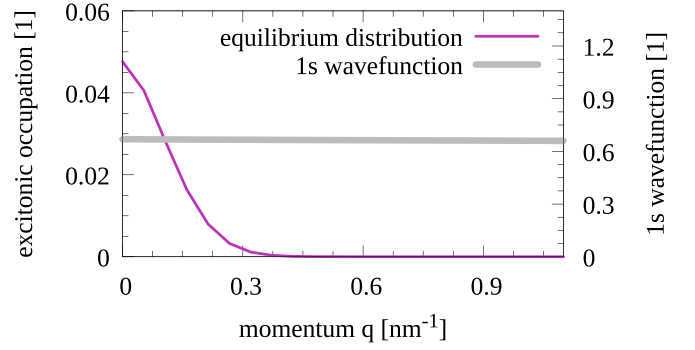


FIG. 2. Equilibrium distribution $N_{\mathbf{Q}}$ at 10 K for a Bohr radius $a_0 \approx 0.2$ nm in momentum space when computed with the full equation (3) exemplarily for TMDC parameters, in comparison to the respective $1s$ wave function $\varphi_{\mathbf{q}}$. The wave function can in very good approximation be estimated as flat in the momentum region of the exciton dynamics.

wavelength:

$$a_0 \ll \lambda_{th}, \quad (17)$$

i.e., the average particle wavelength is large compared to its Bohr radius. We can also express this with regard to temperature and assume $M \approx 1.1 m_{el}$ and $a_0 \approx 2$ nm (typical TMDC values) to get an idea for which temperatures this approximation is valid, e.g., for TMDC excitons:

$$T \ll \frac{\hbar^2}{2Mk_B a_0^2} \approx 98 \text{ K}. \quad (18)$$

This shows that also for experimentally accessible regimes, for instance, in TMDCs, at low temperatures, the analyzed limit remains a good approximation over a large parameter range. In addition, translated to momentum space, this approximation implies that the wave function can be considered flat on the momentum scale of the thermalization dynamics, see Fig. 2. This allows us to approximate $\varphi_{\mathbf{q}} \approx \varphi_{\mathbf{q}+\mathbf{Q}}$ in the appearing overlap integrals in the scattering matrices in Eqs. (6), (B1), and (B2), i.e., we set

$$\sum_{\mathbf{q}} (\varphi_{\mathbf{q}})^* \varphi_{\mathbf{q}-\beta\mathbf{Q}} \approx 1, \quad (19)$$

and approximate other overlap integrals accordingly. In physical terms this means that we neglect that the overlap integrals are slightly smaller than 1, as this is a small effect in this regime. We carefully checked that in the limit of Eq. (17), the full numerics [39] give very similar results with and without this assumption, see Appendix C.

If we apply this approximation to all scattering tensors, the long expressions for the overlaps of four and six wave functions in Eqs. (B1) and (B2) can be reduced to analytically solvable expressions of the form $\sum_{\mathbf{q}} |\varphi_{\mathbf{q}}|^4$ and $\sum_{\mathbf{q}} |\varphi_{\mathbf{q}}|^6$, respectively. This allows us to give analytic expressions depending on a_0 for the overlaps, which we introduce as the dimension-dependent abbreviations $\mathcal{F}^d, \mathcal{B}^d, d \in \{2, 3\}$, see Appendix D. These abbreviations allow for a dimension-invariant derivation, making use of the fact that after the

approximation, Eq. (19), the integrals over the wave function give only an analytically computable factor and a dependence of the Bohr radius a_0 , for the fermionic term a_0^d , and for the

exchange term even $(a_0^d)^2$. We furthermore identify the exciton density \bar{n} , Eq. (7). This allows us to significantly simplify the main equation to

$$\begin{aligned} \partial_t N_{\mathbf{Q}} \approx & \frac{2\pi}{\hbar} \sum_{\mathbf{Q}'\alpha\pm} |g_{\mathbf{Q}'-\mathbf{Q}}^{c\alpha} - g_{\mathbf{Q}'-\mathbf{Q}}^{v\alpha}|^2 \\ & \times \left[\left(\frac{1}{2} \pm \frac{1}{2} + n_{|\mathbf{Q}'-\mathbf{Q}|}^\alpha \right) \delta(\mathcal{E}_{\mathbf{Q}'} - \mathcal{E}_{\mathbf{Q}} \pm \hbar\omega_{|\mathbf{Q}'-\mathbf{Q}|}^\alpha) N_{\mathbf{Q}'} - \left(\frac{1}{2} \pm \frac{1}{2} + n_{|\mathbf{Q}'-\mathbf{Q}|}^\alpha \right) \delta(\mathcal{E}_{\mathbf{Q}'} - \mathcal{E}_{\mathbf{Q}} \mp \hbar\omega_{|\mathbf{Q}'-\mathbf{Q}|}^\alpha) N_{\mathbf{Q}} \right. \\ & \left. + (N_{\mathbf{Q}'} N_{\mathbf{Q}} - 2\bar{n} a_0^d \mathcal{F}^d (N_{\mathbf{Q}'} + N_{\mathbf{Q}}) + (\bar{n} a_0^d)^2 \mathcal{B}^d) (\delta(\mathcal{E}_{\mathbf{Q}} - \mathcal{E}_{\mathbf{Q}'} + \hbar\omega_{|\mathbf{Q}'-\mathbf{Q}|}^\alpha) - \delta(\mathcal{E}_{\mathbf{Q}} - \mathcal{E}_{\mathbf{Q}'} - \hbar\omega_{|\mathbf{Q}'-\mathbf{Q}|}^\alpha)) \right]. \quad (20) \end{aligned}$$

Note that this approximate form, Eq. (20), is—as is the full equation, Eq. (3)—density conserving, which can be seen when executing the sum over all momenta ($\sum_{\mathbf{Q}} \partial_t N_{\mathbf{Q}}$). For the nonlinearities, the density is conserved for each term separately, simply because the sum $\sum_{\mathbf{Q}\mathbf{Q}'\alpha} \delta(\mathcal{E}_{\mathbf{Q}} - \mathcal{E}_{\mathbf{Q}'} + \hbar\omega_{|\mathbf{Q}'-\mathbf{Q}|}^\alpha) - \delta(\mathcal{E}_{\mathbf{Q}} - \mathcal{E}_{\mathbf{Q}'} - \hbar\omega_{|\mathbf{Q}'-\mathbf{Q}|}^\alpha) = 0$.

Equation (20) allows for a better understanding of the derived full excitonic scattering equation, Eq. (3). First of all, the second line represents the classical, linear case, which at approaching equilibrium drives the exciton distribution into the classical Maxwell-Boltzmann distribution. The temperature enters here directly via the phononic occupation number $n_{\mathbf{Q}}^\alpha(T)$, i.e., the phonon equilibrium Bose distribution; thus the second line of Eq. (20) corresponds to the classical thermalization dynamics in dilute gases [52,67,68]. Above the low-density limit, terms of the order of \bar{n}^2 become relevant, leading to a deviation from the Maxwell-Boltzmann distribution in equilibrium.

The last line of Eq. (20) accounts for these different nonlinearities induced by quantum effects beyond the classical gas dynamics. Evidently, all nonlinearities share the same phonon prefactor and energy-momentum selection rules. The first term, scaling as $N_{\mathbf{Q}'} N_{\mathbf{Q}}$, corresponds to the ideal, bosonic case and is independent of the unitless parameter $\eta = \bar{n} a_0^d$ (it is dependent on the density \bar{n} via the square of the occupation, but not on the Bohr radius, as we will see in the following). In contrast, the corrections due to the fermionic substructure of the excitons are typically scaling in orders of $\bar{n} a_0^d$ [33,35], and it thus is intuitive that also in the case of Eq. (3) those terms depend on this unitless parameter; the occurring nonlinearity with negative sign goes linear in η , the attractive exchange even with the square, η^2 .

Equation (20) also makes a fact visible which will become important in the following: The bosonic, stimulated scattering, i.e., the first nonlinear term, is dependent not only on the occupation $N_{\mathbf{Q}}$ itself but also on the occupation of the respective scattering partner $N_{\mathbf{Q}'}$, with the momentum \mathbf{Q}' determined by the Fermi selection rules [last line in Eq. (20)]. For the stimulated scattering, especially the scattering to the ground state (the $\mathbf{Q} = 0$ mode) this is decisive. In the following we treat the scattering momentum provided by the phonons to fill the ground state as a key parameter for the classification of the exciton thermalization as of bosonic or fermionic tendency. We denote the respective

momentum for scattering to the ground state \mathbf{Q}_{phon} . Taking the phonon dispersion into account, for inelastic, optical phonon scattering, this momentum is comparatively large, typically in the range of $\mathbf{Q}_{\text{phon}} \approx 1 \text{ nm}^{-1}$ for TMDC monolayers, while acoustic phonons show angular dependent, yet significantly smaller momenta in the range $\mathbf{Q}_{\text{phon}} \approx 0.05 - 0.1 \text{ nm}^{-1}$ [47,48,53,69]. As a consequence, the occupation of the modes that provide the scattering to the ground state are significantly higher populated for acoustic phonons than for optical ones, as is illustrated for a monolayer MoSe₂ at $T = 10 \text{ K}$ in Fig. 3. This is important, since the fermionic Pauli repulsion occurs independent of this specific occupation $N_{\mathbf{Q}_{\text{phon}}}$ but sums over all occupations and is thus independent of the scattering momentum, i.e., the second and third

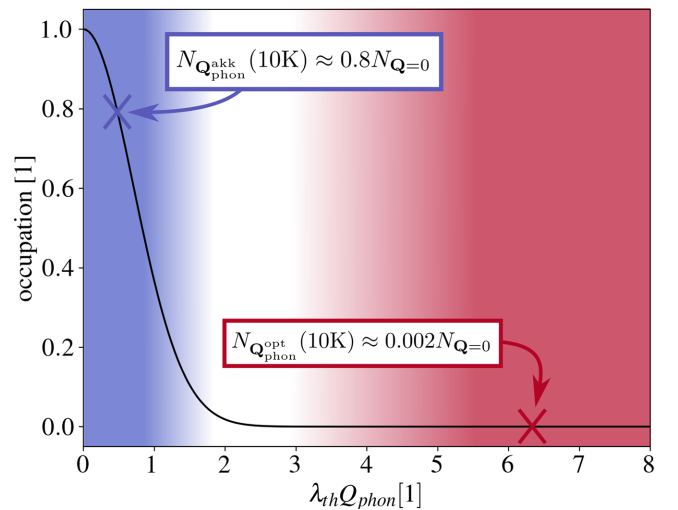


FIG. 3. Visualization of the occupation $N_{\mathbf{Q}'}$ of the scattering partner for the lowest $Q = 0$ mode, compared to $N_{\mathbf{Q}=0}$, see Eq. (20), but also in the main equation, Eq. (3). We show exemplary values at $T = 10 \text{ K}$, the lower the temperature, the lower also the occupation of the scattering partners. We can see that for acoustic, i.e., rather elastic phonon scattering, the occupation of the scattering partner is high enough that the bosonic nonlinearity can win over the fermionic term in Eq. (20). For optical scattering the occupation of the exciton state that scatters to the ground mode is almost unoccupied. Thus, the repulsion will win over the stimulated scattering, as it is independent of this occupation.

nonlinearities in Eq. (3), scaling with $\bar{n}a_0^d$ and $(\bar{n}a_0^d)^2$, and do not rely on high values of the occupation $N_{\mathbf{Q}_{\text{phon}}}$ compared to the occupation of the ground mode, $N_{\mathbf{Q}=0}$. Thus, for dominant optical, i.e., inelastic phonon scattering, the excitonic thermalization cannot be bosonic, as we will show in more detail in the following.

B. Small deviations from the classical Maxwell-Boltzmann limit

In the following, we focus on small deviations from the classical thermalization, as we are only interested in the first deviation from the classical thermalization. Thorough numerical studies [39] always suggested monotonous behavior of bosonic or fermionic deviations with density for a set of exciton mass and temperature. It is therefore sufficient to

concentrate on densities where the equilibrated occupation shows the first small deviations $\delta N_{\mathbf{Q}} = N_{\mathbf{Q}} - N_{\mathbf{Q}}^{\text{MB}}$ compared to a classical thermalization distribution $N_{\mathbf{Q}}^{\text{MB}}$ (which follows a Maxwell-Boltzmann statistics). At even higher densities, this trend set by the first deviations is only intensified, resulting in stronger deviations of the same kind (bosonic or fermionic compared to a classical distribution). This allows us to write an equation of this deviation in leading order of $\delta N_{\mathbf{Q}}$. In the Boltzmann limit, the occupations for a given exciton density \bar{n} read for arbitrary dimension d

$$N_{\mathbf{Q}}^{\text{MB}} \approx (2\pi^{\frac{1}{2}}\lambda_{th})^d \bar{n} e^{-\lambda_{th}^2 Q^2}. \quad (21)$$

The prefactor can be obtained by using the definition of the exciton density \bar{n} , Eq. (7), for normalization. Assuming $\delta N_{\mathbf{Q}}$ to be small allows us to rewrite Eq. (20) to

$$\begin{aligned} \partial_t(N_{\mathbf{Q}}^{\text{MB}} + \delta N_{\mathbf{Q}}) &\approx \frac{2\pi}{\hbar} \sum_{\mathbf{Q}'\alpha\pm} |g_{\mathbf{Q}'-\mathbf{Q}}^{\alpha} - g_{\mathbf{Q}'-\mathbf{Q}}^{\nu\alpha}|^2 \\ &\times \left[\left(\frac{1}{2} \pm \frac{1}{2} + n_{|\mathbf{Q}-\mathbf{Q}'|}^{\alpha} \right) \delta(\mathcal{E}_{\mathbf{Q}} - \mathcal{E}_{\mathbf{Q}} \pm \hbar\omega_{|\mathbf{Q}-\mathbf{Q}'|}^{\alpha}) N_{\mathbf{Q}}^{\text{MB}} - \left(\frac{1}{2} \pm \frac{1}{2} + n_{|\mathbf{Q}-\mathbf{Q}'|}^{\alpha} \right) \delta(\mathcal{E}_{\mathbf{Q}} - \mathcal{E}_{\mathbf{Q}} \mp \hbar\omega_{|\mathbf{Q}-\mathbf{Q}'|}^{\alpha}) N_{\mathbf{Q}}^{\text{MB}} \right. \\ &+ \left(\frac{1}{2} \pm \frac{1}{2} + n_{|\mathbf{Q}-\mathbf{Q}'|}^{\alpha} \right) \delta(\mathcal{E}_{\mathbf{Q}} - \mathcal{E}_{\mathbf{Q}} \pm \hbar\omega_{|\mathbf{Q}-\mathbf{Q}'|}^{\alpha}) \delta N_{\mathbf{Q}} - \left(\frac{1}{2} \pm \frac{1}{2} + n_{|\mathbf{Q}-\mathbf{Q}'|}^{\alpha} \right) \delta(\mathcal{E}_{\mathbf{Q}} - \mathcal{E}_{\mathbf{Q}} \mp \hbar\omega_{|\mathbf{Q}-\mathbf{Q}'|}^{\alpha}) \delta N_{\mathbf{Q}} \\ &+ ((N_{\mathbf{Q}}^{\text{MB}} N_{\mathbf{Q}}^{\text{MB}} + \delta N_{\mathbf{Q}} N_{\mathbf{Q}}^{\text{MB}} + N_{\mathbf{Q}}^{\text{MB}} \delta N_{\mathbf{Q}} + \delta N_{\mathbf{Q}} \delta N_{\mathbf{Q}}) - 2\bar{n}a_0^d \mathcal{F}^d [N_{\mathbf{Q}}^{\text{MB}} + \delta N_{\mathbf{Q}} + N_{\mathbf{Q}}^{\text{MB}} + \delta N_{\mathbf{Q}}] + \bar{n}a_0^d)^2 \mathcal{B}^d \\ &\left. \times (\delta(\mathcal{E}_{\mathbf{Q}} - \mathcal{E}_{\mathbf{Q}} + \hbar\omega_{|\mathbf{Q}-\mathbf{Q}'|}^{\alpha}) - \delta(\mathcal{E}_{\mathbf{Q}} - \mathcal{E}_{\mathbf{Q}} - \hbar\omega_{|\mathbf{Q}-\mathbf{Q}'|}^{\alpha})) \right]. \quad (22) \end{aligned}$$

First of all, $\partial_t(N_{\mathbf{Q}}^{\text{MB}}) = 0$ (the equilibrated classical distribution is constant in time). Besides, the first two terms of Eq. (22) cancel each other out, as can be directly seen when inserting Eq. (21), and which has to be the case, as the Boltzmann statistics solve the classical Boltzmann scattering equation [17,52,71]. Then, the leading order is identified, with $1 \gg N_{\mathbf{Q}} \gg N_{\mathbf{Q}} N_{\mathbf{Q}} \gg \delta N_{\mathbf{Q}} \gg N_{\mathbf{Q}} \delta N_{\mathbf{Q}} \gg \delta N_{\mathbf{Q}} \delta N_{\mathbf{Q}}$, which gives

$$\begin{aligned} \partial_t(\delta N_{\mathbf{Q}}) &\approx \frac{2\pi}{\hbar} \sum_{\mathbf{Q}'\alpha\pm} |g_{\mathbf{Q}'-\mathbf{Q}}^{\alpha} - g_{\mathbf{Q}'-\mathbf{Q}}^{\nu\alpha}|^2 \\ &\times \left[\left(\frac{1}{2} \pm \frac{1}{2} + n_{|\mathbf{Q}-\mathbf{Q}'|}^{\alpha} \right) \delta(\mathcal{E}_{\mathbf{Q}} - \mathcal{E}_{\mathbf{Q}} \pm \hbar\omega_{|\mathbf{Q}-\mathbf{Q}'|}^{\alpha}) \delta N_{\mathbf{Q}} - \left(\frac{1}{2} \pm \frac{1}{2} + n_{|\mathbf{Q}-\mathbf{Q}'|}^{\alpha} \right) \delta(\mathcal{E}_{\mathbf{Q}} - \mathcal{E}_{\mathbf{Q}} \mp \hbar\omega_{|\mathbf{Q}-\mathbf{Q}'|}^{\alpha}) \delta N_{\mathbf{Q}} \right. \\ &\left. + (N_{\mathbf{Q}}^{\text{MB}} N_{\mathbf{Q}}^{\text{MB}} - 2\bar{n}a_0^d \mathcal{F}^d [(N_{\mathbf{Q}}^{\text{MB}}) + (N_{\mathbf{Q}}^{\text{MB}})] + (\bar{n}a_0^d)^2 \mathcal{B}^d) (\delta(\mathcal{E}_{\mathbf{Q}} - \mathcal{E}_{\mathbf{Q}} + \hbar\omega_{|\mathbf{Q}-\mathbf{Q}'|}^{\alpha}) - \delta(\mathcal{E}_{\mathbf{Q}} - \mathcal{E}_{\mathbf{Q}} - \hbar\omega_{|\mathbf{Q}-\mathbf{Q}'|}^{\alpha})) \right]. \quad (23) \end{aligned}$$

The tendency of $\delta N_{\mathbf{Q}}$ towards a distribution that is more fermionic (negative at $\mathbf{Q} = 0$) or bosonic (positive at $\mathbf{Q} = 0$) than the classical equation will essentially depend on the sign of the inhomogeneous part of Eq. (23), which is why we can focus on the inhomogeneous source terms of the equation $\partial_t(\delta N_{\mathbf{Q}})$ and thus neglect the homogenous part, i.e., the contributions linear in $\delta N_{\mathbf{Q}}$ on the right side, which, after inserting Eq. (21), gives

$$\begin{aligned} \partial_t(\delta N_{\mathbf{Q}}) &\approx \frac{2\pi}{\hbar} \sum_{\alpha\mathbf{Q}'} |g_{\mathbf{Q}'-\mathbf{Q}}^{\alpha} - g_{\alpha,\mathbf{Q}'-\mathbf{Q}}^{\nu\alpha}|^2 \pi^2 \bar{n}^2 ((2\pi^{\frac{1}{2}}\lambda_{th})^{2d} e^{-\lambda_{th}^2 Q^2} e^{-\lambda_{th}^2 Q^2} - 2(2\pi^{\frac{1}{2}}\lambda_{th})^d a_0^d \mathcal{F}^d (e^{-\lambda_{th}^2 Q^2} + e^{-\lambda_{th}^2 Q^2}) + (a_0^d)^2 \mathcal{B}^d) \\ &\times (\delta(\mathcal{E}_{\mathbf{Q}} - \mathcal{E}_{\mathbf{Q}} + \hbar\omega_{|\mathbf{Q}-\mathbf{Q}'|}^{\alpha}) - \delta(\mathcal{E}_{\mathbf{Q}} - \mathcal{E}_{\mathbf{Q}} - \hbar\omega_{|\mathbf{Q}-\mathbf{Q}'|}^{\alpha})). \quad (24) \end{aligned}$$

In Eq. (24), all three terms appear consistently in second order in \bar{n} . However, the first term, the ideal bosonic nonlinearity, is entirely independent of the Bohr radius a_0 and just depends on the thermal wavelength λ_{th} , i.e., it will be more important at low temperatures and for small excitonic

masses, as one would expect for ideal bosons. The fermionic corrections, however, depend on the Bohr radius a_0 . In order to predict the sign of the nonlinearity, Eq. (24), with respect to the ground state, we compute the equation for the occupation at $\mathbf{Q} = 0$, which allows us to eliminate the $\sum_{\mathbf{Q}}$

by the Fermi rule δ functions. This is in principle possible for arbitrary phonon dispersions, as long as one has an analytic expression for the phonon energy $\hbar\omega^\alpha$. To give an example, we illustrate it here for a monolayer TMDC, where typically, for optical phonons, one can assume zeroth-order deformation potential, i.e., $\hbar\omega^{\text{opt}} \approx E_{\text{opt}} = \text{const.}$ [53,69], and thus $Q_{\text{phon}}^{\text{opt}} = \sqrt{\frac{2M}{\hbar^2} E_{\text{opt}}}$, while for acoustical phonons, one

can typically assume first-order deformation potential, thus a linear dispersion $\hbar\omega^{\text{ack}} \approx kc_{\text{ack}}$ [53,69], and hence $Q_{\text{phon}}^{\text{ack}} = \frac{2M}{\hbar^2} c_{\text{ack}}$. This is, however, only to give an example; in other materials, different phonon modes are important and hence the values of the momentum are also different. In the following we only assume that we obtained a Q_{phon}^α from the Dirac δ and eliminated the $\sum_{\mathbf{Q}}$ in Eq. (24). This gives

$$\partial_t(\delta N_{\mathbf{Q}=0}) = \frac{L^d}{\hbar\pi^{d-2}} \sum_{\alpha} Q_{\text{phon}}^\alpha |g_{Q_{\text{phon}}^\alpha}^{c\alpha} - g_{Q_{\text{phon}}^\alpha}^{v\alpha}|^2 \bar{n}^2 \left((2\pi^{\frac{1}{2}} \lambda_{th})^{2d} e^{-\lambda_{th}^2 (Q_{\text{phon}}^\alpha)^2} - 2(2\pi^{\frac{1}{2}} \lambda_{th})^d a_0^d \mathcal{F}^d (e^{-\lambda_{th}^2 (Q_{\text{phon}}^\alpha)^2} + 1) + (a_0^d)^2 \mathcal{B}^d \right), \quad (25)$$

or, in 2D, i.e., for $d = 2$,

$$\partial_t(\delta N_{\mathbf{Q}=0}) = \frac{L^2}{\hbar} \sum_{\alpha} Q_{\text{phon}}^\alpha |g_{Q_{\text{phon}}^\alpha}^{c\alpha} - g_{Q_{\text{phon}}^\alpha}^{v\alpha}|^2 16\pi^2 \bar{n}^2 \left(\lambda_{th}^4 e^{-\lambda_{th}^2 (Q_{\text{phon}}^\alpha)^2} - \frac{8}{5} \lambda_{th}^2 a_0^2 (e^{-\lambda_{th}^2 (Q_{\text{phon}}^\alpha)^2} + 1) + a_0^4 \right), \quad (26)$$

$\equiv \lambda_{th}^4 f_{2D}^\alpha \left(\frac{a_0}{\lambda_{th}}, \lambda_{th} Q_{\text{phon}}^\alpha \right)$

and in 3D, i.e., $d = 3$,

$$\partial_t(\delta N_{\mathbf{Q}=0}) = \frac{L^3}{\hbar} \sum_{\alpha} Q_{\text{phon}}^\alpha |g_{Q_{\text{phon}}^\alpha}^{c\alpha} - g_{Q_{\text{phon}}^\alpha}^{v\alpha}|^2 16\pi^2 \bar{n}^2 \left(64\lambda_{th}^6 \pi e^{-\lambda_{th}^2 (Q_{\text{phon}}^\alpha)^2} - 264\sqrt{\pi} a_0^3 \lambda_{th}^3 (e^{-\lambda_{th}^2 (Q_{\text{phon}}^\alpha)^2} + 1) + a_0^6 \frac{4199}{8} \right). \quad (27)$$

$\equiv \lambda_{th}^6 f_{3D}^\alpha \left(\frac{a_0}{\lambda_{th}}, \lambda_{th} Q_{\text{phon}}^\alpha \right)$

IV. RESULTS IN UNITLESS PARAMETERS

A. Individual phonon branches

In Eq. (3), typically, both acoustic and optical phonon modes contribute to the index α . In the following we treat the phononic modes individually to determine the sign of the combined nonlinearities of each phononic mode on the energetically lowest excitonic state at $\mathbf{Q} = 0$. The border $f_d^\alpha \left(\frac{a_0}{\lambda_{th}}, \lambda_{th} Q_{\text{phon}}^\alpha \right) = 0$ between fermionic and bosonic behavior is determined by setting $\delta N_{\mathbf{Q}=0} = 0$:

$$0 = \left((2\pi^{\frac{1}{2}} \lambda_{th})^{2d} e^{-\lambda_{th}^2 (Q_{\text{phon}}^\alpha)^2} - 2a_0^d \mathcal{F}^d (2\pi^{\frac{1}{2}} \lambda_{th})^d \right. \\ \left. \times (e^{-\lambda_{th}^2 (Q_{\text{phon}}^\alpha)^2} + 1) + (a_0^d)^2 \mathcal{B}^d \right). \quad (28)$$

When divided by $(\lambda_{th}^d)^2$, we can rewrite Eqs. (26) and (27) to

$$f_{2D}^\alpha \left(\frac{a_0}{\lambda_{th}}, \lambda_{th} Q_{\text{phon}}^\alpha \right) \\ = 16e^{-\lambda_{th}^2 (Q_{\text{phon}}^\alpha)^2} - \frac{32}{5} \frac{a_0^2}{\lambda_{th}^2} (e^{-\lambda_{th}^2 (Q_{\text{phon}}^\alpha)^2} + 1) + \frac{a_0^4}{\lambda_{th}^4}, \quad (29)$$

and for $d = 3$,

$$f_{3D}^\alpha \left(\frac{a_0}{\lambda_{th}}, \lambda_{th} Q_{\text{phon}}^\alpha \right) \\ = \pi e^{-\lambda_{th}^2 (Q_{\text{phon}}^\alpha)^2} - \frac{33}{8} \sqrt{\pi} \frac{a_0^3}{\lambda_{th}^3} (e^{-\lambda_{th}^2 (Q_{\text{phon}}^\alpha)^2} + 1) \\ + \frac{a_0^6}{\lambda_{th}^6} \frac{4199}{512}. \quad (30)$$

Interestingly, only the dimensionless parameters $\frac{a_0}{\lambda_{th}}$ and $\lambda_{th} Q_{\text{phon}}$ (or, as later shown, equivalently $a_0 Q_{\text{phon}}$) determine the dynamics. Figure 4 is a plot of the sign of Eqs. (29) and (30) over the unitless parameters $\frac{a_0}{\lambda_{th}}$ and $\lambda_{th} Q_{\text{phon}}$. This plot in principle applies in general for different semiconductor materials, as long as phonon scattering of two- or three-dimensional semiconductor excitons dominates the dynamics. For both two- and three-dimensional excitons, one can see that as expected, the excitons become more bosonic with decreasing Bohr radius a_0 , with 3D excitons being even more sensitive towards this radius, which makes sense as it enters the equation in powers of a_0^d , thus more dimensions d make the dependency stronger.

In Appendix E we show that the limiting case of ideal bosonic behavior is included, which makes sense mathematically, when setting $a_0 = 0$ in Eqs. (29) and (30), only the first term prevails, which stands for bosonic stimulated scattering to the ground state similar to the behavior of ideal bosons. In the same Appendix we also provide log plots showing that this limiting case is only approached very slowly; thus for all realistic Bohr radii we always have strong contributions from the fermionic corrections.

In order to relate our findings to experimentally reasonable values for the unitless parameters, we exemplarily provide positions in this parameter plane for TMDC excitons, which we estimate to have a Bohr radius of $a_0 = 2$ nm and a mass of $M = 1.1 m_{el}$. This allows us to give exemplary lines for temperature (vertical) and for typical phonon momenta Q_{phon} (the momentum that a typical scattering event requires for scattering to the ground state). It becomes evident from Fig. 4 that optical phonon processes require too large momenta to make bosonic behavior probable, while acoustical phonons are more likely to favor bosonic thermalization. The fact that

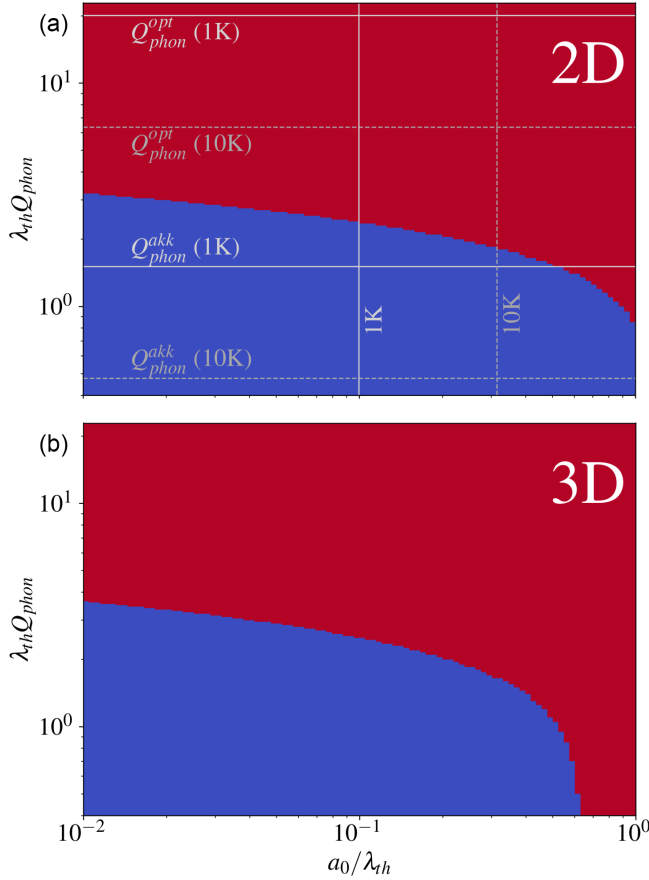


FIG. 4. Plot of the sign of the nonlinearities deciding the thermalization occupation of the ground state as a function of the unitless parameters $\frac{a_0}{\lambda_{th}}$ and $\lambda_{th}Q_{phon}^\alpha$. Blue stands for a positive sign of $f_d^\alpha(\frac{\lambda_{th}}{a_0}, \lambda_{th}Q_{phon}^\alpha)$, indicating bosonic thermalization behavior, and red stands for a negative sign, respectively indicating fermionic behavior compared to the classical distribution. (a) 2D case, Eq. (29). The gray lines in the 2D plot show temperatures and $\lambda_{th}Q_{phon}^\alpha$ values for typical TMDC parameters, i.e., $a_0 = 2$ nm and $M = 1.1 m_{el}$, in order to give an orientation in the parameter plane. (b) Same plot for the 3D case, Eq. (30). (Above $\frac{a_0}{\lambda_{th}} > 1$ in principle there is another parameter range with positive sign; however, the approximations we made require $a_0 \ll \lambda_{th}$, and thus we show only the region that is in accordance with this approximation).

the bosonic first term in Eqs. (29) and (30) only for very small scattering momenta dominates the second term, its fermionic counterpart is here encoded in the exponential function we inserted for the occupation of the scattering partner $N_{Q_{phon}^\alpha}$. Large momenta between the excitonic states for optical phonon scattering lead to small occupation of the scattering partner, as already shown in Fig. 3. Inelastic, optical phonon scattering therefore hinders bosonic thermalization. This is in very good agreement with our findings from the full numerics [39].

A shortcoming of the plot in Fig. 4 is that it is not very intuitive to read temperature dependencies from it. We therefore provide another set of equations, where λ_{th} is only on one axis and thus the temperature dependence can be seen more directly. We will see that it does not alter our main finding that optical phonon modes (or, more gener-

ally, inelastic phonon scattering) inhibit stimulated scattering effects.

The whole expressions of Eqs. (26) and (27) divided by $(a_0^2)^d$ read for 2D

$$g_{2D}^\alpha \left(\frac{\lambda_{th}}{a_0}, a_0 Q_{phon}^\alpha \right) = 16 \frac{\lambda_{th}^4}{a_0^4} e^{-\frac{\lambda_{th}^2}{a_0^2} (a_0 Q_{phon}^\alpha)^2} - \frac{32}{5} \frac{\lambda_{th}^2}{a_0^2} \left(e^{-\frac{\lambda_{th}^2}{a_0^2} (a_0 Q_{phon}^\alpha)^2} + 1 \right) + 1 \quad (31)$$

and for 3D

$$g_{3D}^\alpha \left(\frac{\lambda_{th}}{a_0}, a_0 Q_{phon}^\alpha \right) = \pi \frac{\lambda_{th}^6}{a_0^6} e^{-\frac{\lambda_{th}^2}{a_0^2} (a_0 Q_{phon}^\alpha)^2} - \frac{33}{8} \sqrt{\pi} \frac{\lambda_{th}^3}{a_0^3} \left(e^{-\frac{\lambda_{th}^2}{a_0^2} (a_0 Q_{phon}^\alpha)^2} + 1 \right) + \frac{4199}{512}. \quad (32)$$

(Note that we rewrote also the arguments of the exponentials in order to express everything with respect to the same unitless parameters.) Figure 5 is a plot of the sign of Eqs. (31) and (32) as a function of the unitless parameters $\frac{\lambda_{th}}{a_0}$ and $a_0 Q_{phon}^\alpha$. From the plot we can see that in order to expect bosonic signatures, the temperature has to be chosen low enough that for the respective particle mass, λ_{th} can compensate the Bohr radius a_0 . Furthermore, one requires values of $Q_{phon}^\alpha \ll \frac{1}{a_0}$ for 2D excitons or $Q_{phon}^\alpha \ll \frac{1}{2a_0}$ in the 3D case. Such low scattering momenta typically can only be provided by acoustic, quasielastic phonon scattering. For larger Q_{phon}^α , the fermionic nonlinearity dominates [to be precise, the $+1$ next to the respective exponential function wins for too large values of Q_{phon}^α in Eq. (31)]. Interestingly, 3D excitons are even more temperature sensitive, with only a comparatively small window of temperatures apparently allowing for bosonic behavior if the dominant phonon process is elastic enough.

For TMDC excitons, we can again estimate $a_0 = 2$ nm and $M = 1.1 m_{el}$ and give exemplary lines for temperature (vertical) and for typical phonon momenta Q_{phon}^α (the momentum that a typical scattering event requires for scattering to the ground state). For the example of TMDC excitons, temperatures between 1 and 10 K look promising for acoustic phonon branches to give positive values, i.e., dominant bosonic signatures. As discussed earlier, optical phonon scattering to the ground state requires much larger momenta, since those scattering processes are much less elastic. The Q_{phon}^{opt} are thus typically one order of magnitude larger than for the acoustic branches, at least in the monolayer [47,48]. They will thus contribute with a negative sign and lead to a fermionic thermalization behavior.

B. Sum over phonon branches

In the more realistic case of taking all phonon branches into account that are relevantly contributing to the scattering process, we have to consider the sum over α in Eq. (25) and thus get prefactors for the contributions from the different branches, which depend on the Q_{phon}^α of the respective phonon

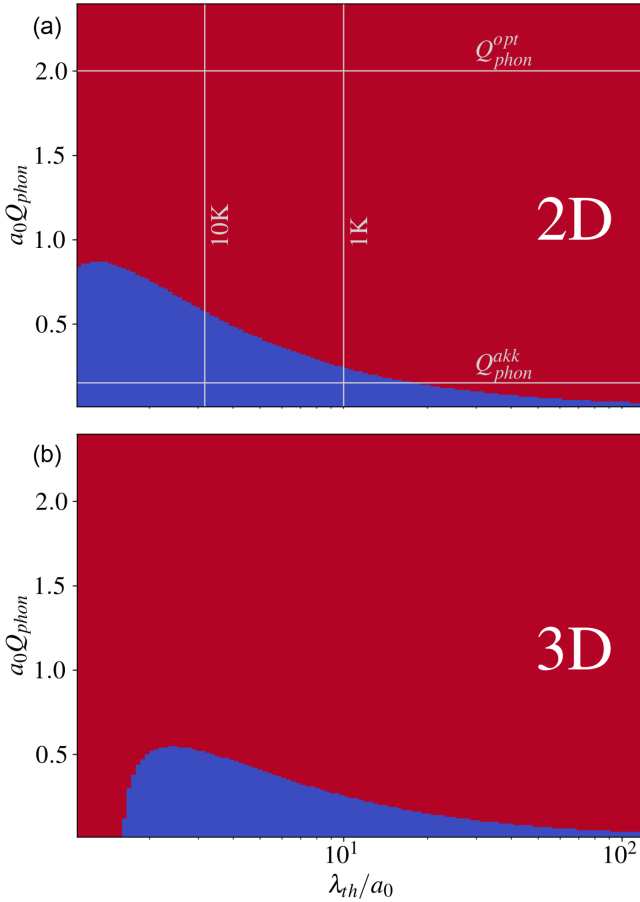


FIG. 5. Plot of the sign of the nonlinearities deciding the thermalization occupation of the ground state as a function of the unitless parameters $\frac{\lambda_{th}}{a_0}$ and $a_0 Q_{\text{phon}}^\alpha$. Blue stands for a positive sign of $g_d^\alpha(\frac{\lambda_{th}}{a_0}, a_0 Q_{\text{phon}}^\alpha)$, indicating bosonic thermalization behavior, and red stands for a negative sign, respectively indicating fermionic behavior compared to the classical distribution. (a) 2D case, Eq. (31). The gray lines show temperatures and $a_0 Q_{\text{phon}}$ values for typical TMDC parameters for orientation, i.e., $a_0 = 2$ nm and $M = 1.1 m_{el}$. (b) Same plot for the 3D case, Eq. (32).

mode α , which can be written as

$$h_d\left(\frac{\lambda_{th}}{a_B}, \lambda_{th}\right) = \sum_{\alpha} Q_{\text{phon}}^\alpha |g_{Q_{\text{phon}}^\alpha}^{c,\alpha} - g_{Q_{\text{phon}}^\alpha}^{v,\alpha}|^2 f_d^\alpha\left(\frac{\lambda_{th}}{a_B}, \lambda_{th} Q_{\text{phon}}^\alpha\right). \quad (33)$$

For the example of TMDC excitons, the relation between optical and acoustic phonon scattering branches is

$$Q_{\text{phon}}^{\text{opt}} |g_{Q_{\text{phon}}^{\text{opt}}}^{c,\text{opt}} - g_{Q_{\text{phon}}^{\text{opt}}}^{v,\text{opt}}|^2 \approx 2000 Q_{\text{phon}}^{\text{akk}} |g_{Q_{\text{phon}}^{\text{akk}}}^{c,\text{akk}} - g_{Q_{\text{phon}}^{\text{akk}}}^{v,\text{akk}}|^2. \quad (34)$$

Due to the mentioned larger values for Q_{phon} and the fact that $g_{Q_{\text{phon}}}^{c,v}$ is significantly larger for the optical phonons, the prefactor $Q_{\text{phon}} |g_{Q_{\text{phon}}}^{c,\alpha} - g_{Q_{\text{phon}}}^{v,\alpha}|^2$, for instance, is around 2000 times larger than for the acoustical branch in a TMDC monolayer [47,48,51]. This also applies for the linear equation; however, there the acoustic phonons become important once the $n_Q^\alpha \gg 1$, while the optical mode freezes out [52,53,67]. However, the nonlinear terms are not directly dependent on

temperature; thus for the nonlinearity, optical phonon modes will probably always dominate, at least in monolayer TMDCs.

van der Waals heterostructures of TMDCs and excitons in other kinds of semiconductors may show different behavior if the optical phonon modes are absent, or less dominant. Our study suggests that the macroscopic occupation of the lowest state becomes more probable in systems with dominating acoustic phonons. This is supported by the full numerical solution of Eq. (3). If we simulate the thermalization for only acoustical phonon branches, the thermalization shows a bosonic behavior for much larger Bohr radii, far beyond the TMDC limit of $a_0 = 2$ nm, as can be seen in Fig. 2(b) of Ref. [39].

V. CONCLUSION

We analytically discussed a recently derived equation for the exciton-phonon kinetics [39] above the linear zero density limit. The kinetic equation is microscopically derived from the electron-hole picture, taking the next order in $\eta = \bar{n} a_B^d$ into account, thus going beyond the bosonic commutator relation for those composite particles. In a fully analytic approach, we discussed the effect of Bohr radius, thermal wavelength, and typical phonon scattering momentum on the ground-state occupation to study the question of whether the overall thermalization can be considered bosonic or fermionic and make general statements within a framework of unitless parameters, such as $\frac{a_0}{\lambda_{th}}$, $\lambda_{th} Q_{\text{phon}}$, and $a_0 Q_{\text{phon}}$. Conducting the derivation in a dimension-independent approach allowed us to give predictions for both 2D and 3D exciton systems. As demonstrated before in our numerical study [39], also in the analytical limit we show drastic deviations from a purely bosonic behavior, and show that for typical Bohr radii of around $a_0 = 2$ nm for TMDC excitons, the compound particles cannot be considered bosonic and thus are not likely to show macroscopic occupation effects for the ground state, as long as optical phonon scattering dominates the thermalization dynamics. For significantly smaller Bohr radii, such as, for instance, the reported $a_0 \approx 0.6$ nm for the antiferromagnet van der Waals material NiPS₃ [72], or with absent optical phonon modes at low temperatures, we showed that the respective excitons can be expected to show a bosonic behavior, as the bosonic stimulated scattering in this regime would overcompensate the weaker fermionic Pauli blocking.

ACKNOWLEDGMENTS

We thank Dominik Christiansen, Emil Denning, Aycke Roos, and Marten Richter from TU Berlin; Mirco Troue, Johannes Figueiredo, Lukas Sigl, and Alexander Holleitner from TU München; and Ursula Wurstbauer from University of Münster for fruitful discussions, and gratefully acknowledge support from the Deutsche Forschungsgemeinschaft (DFG) through SFB 951, Project No. 182087777, and via Grant No. KN 427/11-2, Project No. 420760124.

APPENDIX A: DERIVATION OF THE EXCITONIC SCATTERING EQUATION

The excitonic Boltzmann scattering equation, Eq. (3) of the main manuscript, was derived thoroughly in the Supplemental

Material of Ref. [39]. We repeat the most important steps of this derivation here for completeness. The starting point of the derivation is the fundamental electronic semiconductor Hamiltonian [44], Eq. (2) of the main manuscript, where all interactions are introduced with respect to the actual carriers $\lambda^{(\dagger)} \in \{c^{(\dagger)}, v^{(\dagger)}\}$, i.e., the electrons in conduction and valence band. In our analysis we focus on the dynamics of the exciton occupation $N_{\mathbf{Q}}^v$, which we define as a function of these elementary electron and hole operators in Eq. (1) of the main manuscript, where ν denotes the exciton state (we later focus on $\nu = 1s$) and \mathbf{Q} the center-of-mass wave number. This description in the excitonic basis is possible via application of the Wannier equation [35,65]

$$\frac{\hbar^2 \mathbf{q}^2}{2\mu} \varphi_{\mathbf{q}}^v + \sum_{\mathbf{k}} V_{\mathbf{k}} \varphi_{\mathbf{q}+\mathbf{k}}^v = E^v \varphi_{\mathbf{q}}^v, \quad (\text{A1})$$

and by introducing center-of-mass momenta \mathbf{Q} and relative momenta \mathbf{q} ,

$$\mathbf{Q}' = \mathbf{k}_1 - \mathbf{k}_2 \quad \mathbf{Q} = \mathbf{k}_4 - \mathbf{k}_3 \quad (\text{A2})$$

$$\mathbf{q}' = \tilde{\alpha} \mathbf{k}_2 + \tilde{\beta} \mathbf{k}_1 \quad \mathbf{q} = \tilde{\alpha} \mathbf{k}_3 + \tilde{\beta} \mathbf{k}_4 \quad (\text{A3})$$

$$\mathbf{k}_2 = \mathbf{q}' - \tilde{\beta} \mathbf{Q}' \quad \mathbf{k}_3 = \mathbf{q} - \tilde{\beta} \mathbf{Q} \quad (\text{A4})$$

$$\mathbf{k}_1 = \mathbf{q}' + \tilde{\alpha} \mathbf{Q}' \quad \mathbf{k}_4 = \mathbf{q} + \tilde{\alpha} \mathbf{Q}, \quad (\text{A5})$$

where $\tilde{\alpha} = \frac{m_e}{m_e + m_h}$ and $\tilde{\beta} = \frac{m_h}{m_e + m_h}$ give the relative mass of electron and hole. To obtain the dynamics of the exciton occupation, Eq. (1), the Heisenberg equation of motion for the following set of electron and hole operators is computed with respect to the fundamental electronic Hamiltonian, Eq. (2):

$$\begin{aligned} i\hbar \partial_t \langle c_{\mathbf{k}_1}^\dagger v_{\mathbf{k}_2} v_{\mathbf{k}_3}^\dagger c_{\mathbf{k}_4} \rangle &= (\epsilon_{\mathbf{k}_4}^c - \epsilon_{\mathbf{k}_1}^c + \epsilon_{\mathbf{k}_2}^v - \epsilon_{\mathbf{k}_3}^v) \langle c_{\mathbf{k}_1}^\dagger v_{\mathbf{k}_2} v_{\mathbf{k}_3}^\dagger c_{\mathbf{k}_4} \rangle - \sum_{\mathbf{q}} V_{\mathbf{q}} (\langle c_{\mathbf{k}_1}^\dagger v_{\mathbf{k}_2} v_{\mathbf{k}_3-\mathbf{q}}^\dagger c_{\mathbf{k}_4-\mathbf{q}} \rangle - \langle c_{\mathbf{k}_1+\mathbf{q}}^\dagger v_{\mathbf{k}_2+\mathbf{q}} v_{\mathbf{k}_3}^\dagger c_{\mathbf{k}_4} \rangle) \\ &+ \sum_{\mathbf{K}\alpha} (g_{\mathbf{K}}^{c\alpha} (\langle c_{\mathbf{k}_1}^\dagger v_{\mathbf{k}_2} v_{\mathbf{k}_3}^\dagger c_{\mathbf{k}_4-\mathbf{K}} \rangle (b_{\mathbf{K}}^\alpha + b_{-\mathbf{K}}^{\dagger\alpha}) - \langle c_{\mathbf{k}_1+\mathbf{K}}^\dagger v_{\mathbf{k}_2} v_{\mathbf{k}_3}^\dagger c_{\mathbf{k}_4} \rangle (b_{\mathbf{K}}^\alpha + b_{-\mathbf{K}}^{\dagger\alpha}))) \\ &+ g_{\mathbf{K}}^{v\alpha} (\langle c_{\mathbf{k}_1}^\dagger v_{\mathbf{k}_2-\mathbf{K}} v_{\mathbf{k}_3}^\dagger c_{\mathbf{k}_4} \rangle (b_{\mathbf{K}}^\alpha + b_{-\mathbf{K}}^{\dagger\alpha}) - \langle c_{\mathbf{k}_1}^\dagger v_{\mathbf{k}_2} v_{\mathbf{k}_3+\mathbf{K}}^\dagger c_{\mathbf{k}_4} \rangle (b_{\mathbf{K}}^\alpha + b_{-\mathbf{K}}^{\dagger\alpha}))). \end{aligned} \quad (\text{A6})$$

The first line of Eq. (A6) is later summed up in the excitonic dispersion by utilizing Eqs. (A1) and (A2). In order to close Eq. (A6), for the last two lines, i.e., the phononic interactions, it is necessary to compute another set of Heisenberg equations of motion for the phonon-assisted occupation, as given here exemplarily with

$$\begin{aligned} i\hbar \partial_t \langle c_{\mathbf{k}_1}^\dagger v_{\mathbf{k}_2} v_{\mathbf{k}_3}^\dagger c_{\mathbf{k}_4} b_{\mp\mathbf{K}}^{(\dagger)\alpha} \rangle &= (\epsilon_{\mathbf{k}_4}^c - \epsilon_{\mathbf{k}_1}^c - \epsilon_{\mathbf{k}_3}^v + \epsilon_{\mathbf{k}_2}^v \mp \hbar \omega_{\mp\mathbf{K}}^\alpha) \langle c_{\mathbf{k}_1}^\dagger v_{\mathbf{k}_2} v_{\mathbf{k}_3}^\dagger c_{\mathbf{k}_4} b_{\mp\mathbf{K}}^{(\dagger)\alpha} \rangle \\ &- \sum_{\mathbf{q}} V_{\mathbf{q}} (\langle c_{\mathbf{k}_1}^\dagger v_{\mathbf{k}_2} v_{\mathbf{k}_3-\mathbf{q}}^\dagger c_{\mathbf{k}_4-\mathbf{q}} b_{\mp\mathbf{K}}^{(\dagger)\alpha} \rangle - \langle c_{\mathbf{k}_1+\mathbf{q}}^\dagger v_{\mathbf{k}_2+\mathbf{q}} v_{\mathbf{k}_3}^\dagger c_{\mathbf{k}_4} b_{\mp\mathbf{K}}^{(\dagger)\alpha} \rangle) \\ &+ g_{-\mathbf{K}}^{c\alpha} (\langle c_{\mathbf{k}_1}^\dagger v_{\mathbf{k}_2} v_{\mathbf{k}_3}^\dagger c_{\mathbf{k}_4+\mathbf{K}} \rangle n_{\mathbf{K}}^\alpha - \langle c_{\mathbf{k}_1-\mathbf{K}}^\dagger v_{\mathbf{k}_2} v_{\mathbf{k}_3}^\dagger c_{\mathbf{k}_4} \rangle (1 + n_{\mathbf{K}}^\alpha)) \\ &- g_{-\mathbf{K}}^{v\alpha} (\langle c_{\mathbf{k}_1}^\dagger v_{\mathbf{k}_2} v_{\mathbf{k}_3-\mathbf{K}}^\dagger c_{\mathbf{k}_4} \rangle n_{\mathbf{K}}^\alpha - \langle c_{\mathbf{k}_1}^\dagger v_{\mathbf{k}_2+\mathbf{K}} v_{\mathbf{k}_3}^\dagger c_{\mathbf{k}_4} \rangle (1 + n_{\mathbf{K}}^\alpha)) \\ &\pm (1 + n_{\mathbf{K}}^\alpha - n_{\mathbf{K}}^\alpha) \sum_{\lambda\mathbf{k}} g_{-\mathbf{K}}^{\lambda\alpha} \langle c_{\mathbf{k}_1}^\dagger v_{\mathbf{k}_2} \lambda_{\mathbf{k}-\mathbf{K}}^\dagger \lambda_{\mathbf{k}} v_{\mathbf{k}_3}^\dagger c_{\mathbf{k}_4} \rangle, \end{aligned} \quad (\text{A7})$$

where we made two assumptions. We neglect higher-order phonon-exciton correlations, as they are of fourth order in the phononic coupling element $g_{\mathbf{K}}^{\lambda\alpha}$ [52,55,73]:

$$\langle \lambda_1^\dagger \lambda_2 \lambda_3^\dagger \lambda_4 b_1^\dagger b_2 \rangle \approx \langle \lambda_1^\dagger \lambda_2 \lambda_3^\dagger \lambda_4 \rangle \langle b_1^\dagger b_2 \rangle. \quad (\text{A8})$$

Furthermore, we assume a Markovian reservoir for the phonons, i.e.,

$$\langle b_{\mathbf{K}}^\alpha b_{\mathbf{K}'}^{\dagger\alpha} \rangle \approx (1 + n_{\mathbf{K}}^\alpha) \delta_{\mathbf{K},\mathbf{K}'} \quad \langle b_{\mathbf{K}}^\alpha b_{\mathbf{K}'}^\alpha \rangle \approx 0, \quad (\text{A9})$$

with the phononic occupation given by a standard Bose-Einstein statistics [51,67]

$$n_{\mathbf{K}}^\alpha = \frac{1}{\exp(\frac{\hbar \omega_{\mathbf{K}}^\alpha}{k_B T}) - 1}. \quad (\text{A10})$$

When one transforms Eqs. (A6) and (A7) to the exciton picture, leaves out the last term of Eq. (A7), and solves the set of equations in a Born-Markov framework, one obtains the classical Boltzmann scattering equation for the excitonic occupation, as it was documented many times in literature [17,19,52], and which resembles the classical part of Eq. (3), namely, Eq. (4) of the main manuscript. This equation

describes the phonon-scattering-induced dynamics of excitons, as long as the exciton density is low enough to justify the omission of terms second order in $N_{\mathbf{Q}}^v$. In order to include these second-order terms, it is necessary to compute also the last term in Eq. (A7). To close the equation in terms of the exciton operators in undoped materials, where electrons and holes appear always in pairs, we can expand this expectation value of unequal electron and hole number in terms of the unit operator introduced by Ivanov and Haug [33,35] to the first order:

$$\mathbb{1} = \sum_{\mathbf{k}'} c_{\mathbf{k}'}^\dagger c_{\mathbf{k}'} + v_{\mathbf{k}'} v_{\mathbf{k}'}^\dagger, \quad (\text{A11})$$

which gives

$$\begin{aligned} &\sum_{\lambda\mathbf{k}} g_{-\mathbf{K}}^{\lambda\alpha} \langle c_{\mathbf{k}_1}^\dagger v_{\mathbf{k}_2} \lambda_{\mathbf{k}-\mathbf{K}}^\dagger \lambda_{\mathbf{k}} v_{\mathbf{k}_3}^\dagger c_{\mathbf{k}_4} \rangle \\ &= \sum_{\mathbf{k}\mathbf{k}'} (g_{-\mathbf{K}}^{c\alpha} \langle c_{\mathbf{k}_1}^\dagger v_{\mathbf{k}_2} c_{\mathbf{k}-\mathbf{K}}^\dagger v_{\mathbf{k}'} v_{\mathbf{k}'}^\dagger c_{\mathbf{k}} v_{\mathbf{k}_3}^\dagger c_{\mathbf{k}_4} \rangle \\ &- g_{-\mathbf{K}}^{v\alpha} \langle c_{\mathbf{k}_1}^\dagger v_{\mathbf{k}_2} c_{\mathbf{k}'}^\dagger v_{\mathbf{k}} v_{\mathbf{k}-\mathbf{K}}^\dagger c_{\mathbf{k}'} v_{\mathbf{k}_3}^\dagger c_{\mathbf{k}_4} \rangle). \end{aligned} \quad (\text{A12})$$

Applying again the Born-Markov approximation, the resulting eight-operator quantities then have to be factorized as follows [33,36,74]:

$$\begin{aligned} \langle P_{12}^\dagger P_{34}^\dagger P_{56} P_{78} \rangle &\approx \langle P_{12}^\dagger P_{56} \rangle \langle P_{34}^\dagger P_{78} \rangle + \langle P_{12}^\dagger P_{78} \rangle \langle P_{34}^\dagger P_{56} \rangle \\ &\quad - \langle P_{12}^\dagger P_{58} \rangle \langle P_{34}^\dagger P_{76} \rangle - \langle P_{12}^\dagger P_{76} \rangle \langle P_{34}^\dagger P_{58} \rangle \\ &\quad - \langle P_{14}^\dagger P_{56} \rangle \langle P_{32}^\dagger P_{78} \rangle - \langle P_{14}^\dagger P_{78} \rangle \langle P_{32}^\dagger P_{56} \rangle \\ &\quad + \langle P_{14}^\dagger P_{58} \rangle \langle P_{32}^\dagger P_{76} \rangle + \langle P_{14}^\dagger P_{76} \rangle \langle P_{32}^\dagger P_{58} \rangle, \end{aligned} \quad (\text{A13})$$

where we abbreviated

$$P_{12} = v_{\mathbf{k}_1}^\dagger c_{\mathbf{k}_2}, \quad P_{12}^\dagger = c_{\mathbf{k}_2}^\dagger v_{\mathbf{k}_1}, \quad (\text{A14})$$

and so forth. From Eqs. (A12)–(A14), a long and tedious, but rather straightforward computation is necessary, including, as for the classical case, the transformation to the excitonic basis and a solution in the Markov framework, in analogy to the derivation of the classical Boltzmann equation. Before resulting in the excitonic scattering equation, Eq. (3) of the main manuscript, one last assumption is necessary. As we are interested only in the incoherent scattering of exciton occupations, i.e., we only want the final equation to comprise terms like $N_{\mathbf{Q}}^v$ and $(N_{\mathbf{Q}}^v)^2$, we apply a random phase approximation for the appearing products of each of two exciton operators, e.g.,

$$\langle P_{\mathbf{Q}}^{\dagger,\lambda} P_{\mathbf{k}+\mathbf{K}}^{v'} \rangle \langle P_{\mathbf{k}}^{\dagger,\lambda'} P_{\mathbf{Q}-\mathbf{K}}^v \rangle \approx \delta_{\mathbf{k},\mathbf{Q}-\mathbf{K}} \delta^{\lambda\lambda'} N_{\mathbf{Q}}^\lambda N_{\mathbf{Q}-\mathbf{K}}^v. \quad (\text{A15})$$

In summary, the following assumptions were made throughout the derivation:

(1) The electron-phonon interaction is weak enough to justify a treatment in second-order Born approximation, and

the phonon reservoir is equilibrating on a timescale much faster than the excitons, which justifies the assumption of a Markovian phonon reservoir.

(2) The semiconductor is uncharged, allowing for the omission of trions, which is a necessary condition for the application of the unit operator method by Ivanov and Haug [33,35].

(3) This unit operator method is applied to its first order, resulting in terms of the order $(N_{\mathbf{Q}})^2$. Note that the dimensionless parameter $\eta = \bar{n} a_0^d$ (which we introduced in the main text as dependent on the exciton density \bar{n} and the Bohr radius a_0 in d dimensions) is restricted here to the density regime one order higher in η than in the classical case [33,35]. For even higher densities, our equation is no longer valid. Also, the closer the density gets to the Mott transition, the weaker the exciton picture becomes anyway, and a electron-hole picture might be more appropriate.

(4) Random phase approximation: Coherent, nondiagonal terms in Eq. (A15), as well as biexcitons and the like, are excluded from the equation, as we focus on the incoherent, “long-time” thermalization of the excitons. This implies also that the derived equation is most valuable for long-lived excitons, e.g., dark excitons [75] or interlayer excitons in 2D materials [2,76], where the excitonic lifetime is long enough to allow the exciton to fully thermalize before it recombines.

APPENDIX B: WAVE-FUNCTION OVERLAPS

The wave-function overlaps for the fermionic tensors, Eq. (11), read

$$\begin{aligned} g_{\mathbf{Q}\mathbf{Q},\mathbf{K},\alpha}^{F,\lambda v, v'} &= \sum_{\mathbf{q}} g_{\mathbf{Q}-\mathbf{Q}}^{c\alpha} \left((\varphi_{\mathbf{q}}^\lambda)^* (\varphi_{\mathbf{q}+\tilde{\beta}\mathbf{K}+\tilde{\alpha}\mathbf{Q}-\mathbf{Q}}^{v'})^* \varphi_{\mathbf{q}+\tilde{\beta}(\mathbf{K}-\mathbf{Q})}^{v'} \varphi_{\mathbf{q}-\tilde{\alpha}(\mathbf{Q}-\mathbf{Q})}^v + (\varphi_{\mathbf{q}}^\lambda)^* (\varphi_{\mathbf{q}-\tilde{\alpha}(\mathbf{K}-\mathbf{Q})}^{v'})^* \varphi_{\mathbf{q}-\tilde{\alpha}(\mathbf{K}-\mathbf{Q})}^{v'} \varphi_{\mathbf{q}+\tilde{\beta}(\mathbf{Q}-\mathbf{Q})}^v \right) \\ &\quad - g_{\mathbf{Q}-\mathbf{Q}}^{v\alpha} \left((\varphi_{\mathbf{q}}^\lambda)^* (\varphi_{\mathbf{q}+\tilde{\beta}(\mathbf{K}-\mathbf{Q})}^{v'})^* \varphi_{\mathbf{q}+\tilde{\beta}(\mathbf{K}-\mathbf{Q})}^{v'} \varphi_{\mathbf{q}-\tilde{\alpha}(\mathbf{Q}-\mathbf{Q})}^v + (\varphi_{\mathbf{q}}^\lambda)^* (\varphi_{\mathbf{q}-\tilde{\alpha}\mathbf{K}-\tilde{\beta}\mathbf{Q}+\mathbf{Q}}^{v'})^* \varphi_{\mathbf{q}-\tilde{\alpha}(\mathbf{K}-\mathbf{Q})}^{v'} \varphi_{\mathbf{q}+\tilde{\beta}(\mathbf{Q}-\mathbf{Q})}^v \right), \end{aligned} \quad (\text{B1})$$

and for the exchange tensor, Eq. (13),

$$\begin{aligned} g_{\mathbf{Q}\mathbf{Q},\mathbf{K},\mathbf{K}',\alpha}^{E,\lambda v \lambda' v'} &= \sum_{\mathbf{q}} \left(g_{\mathbf{Q}-\mathbf{Q}}^{c\alpha} (\varphi_{\mathbf{q}}^v)^* (\varphi_{\mathbf{q}+\tilde{\alpha}(\mathbf{Q}-\mathbf{K})}^{\lambda'})^* (\varphi_{\mathbf{q}+\tilde{\beta}\mathbf{K}+\tilde{\alpha}\mathbf{Q}-\mathbf{Q}}^{v'})^* \varphi_{\mathbf{q}+\tilde{\beta}\mathbf{K}-\tilde{\beta}\mathbf{Q}}^{v'} \varphi_{\mathbf{q}+\tilde{\alpha}(\mathbf{Q}-\mathbf{K})}^{\lambda'} \varphi_{\mathbf{q}+\tilde{\alpha}(\mathbf{Q}-\mathbf{Q})}^v \right. \\ &\quad + g_{\mathbf{Q}-\mathbf{Q}'}^{c\alpha} (\varphi_{\mathbf{q}}^v)^* (\varphi_{\mathbf{q}-\mathbf{K}+\tilde{\beta}\mathbf{K}'+\tilde{\alpha}\mathbf{Q}}^{\lambda'})^* (\varphi_{\mathbf{q}-\tilde{\alpha}\mathbf{K}+\mathbf{K}'+\tilde{\alpha}\mathbf{Q}-\mathbf{Q}}^{v'})^* \varphi_{\mathbf{q}+\tilde{\beta}\mathbf{K}'-\tilde{\beta}\mathbf{Q}}^{v'} \varphi_{\mathbf{q}-\tilde{\alpha}(\mathbf{K}-\mathbf{Q})}^{\lambda'} \varphi_{\mathbf{q}-\mathbf{K}+\mathbf{K}'+\tilde{\alpha}(\mathbf{Q}-\mathbf{Q})}^v \\ &\quad - g_{\mathbf{Q}-\mathbf{Q}'}^{v\alpha} (\varphi_{\mathbf{q}}^v)^* (\varphi_{\mathbf{q}-\tilde{\alpha}\mathbf{K}'-\tilde{\beta}\mathbf{Q}+\mathbf{Q}}^{\lambda'})^* (\varphi_{\mathbf{q}+\tilde{\beta}(\mathbf{K}-\mathbf{Q})}^{v'})^* \varphi_{\mathbf{q}+\tilde{\beta}(\mathbf{K}-\mathbf{Q})}^{v'} \varphi_{\mathbf{q}-\tilde{\alpha}\mathbf{K}'+\tilde{\alpha}\mathbf{Q}}^{\lambda'} \varphi_{\mathbf{q}-\tilde{\beta}(\mathbf{Q}-\mathbf{Q})}^v \\ &\quad \left. - g_{\mathbf{Q}-\mathbf{Q}'}^{v\alpha} (\varphi_{\mathbf{q}}^v)^* (\varphi_{\mathbf{q}-\mathbf{K}+\tilde{\beta}\mathbf{K}'-\tilde{\beta}\mathbf{Q}+\mathbf{Q}}^{\lambda'})^* (\varphi_{\mathbf{q}-\tilde{\alpha}\mathbf{K}+\mathbf{K}'-\tilde{\beta}\mathbf{Q}}^{v'})^* \varphi_{\mathbf{q}-\tilde{\beta}(\mathbf{Q}-\mathbf{K})}^{v'} \varphi_{\mathbf{q}-\tilde{\alpha}\mathbf{K}+\tilde{\alpha}\mathbf{Q}}^{\lambda'} \varphi_{\mathbf{q}-\mathbf{K}+\mathbf{K}'-\tilde{\beta}(\mathbf{Q}-\mathbf{Q})}^v \right). \end{aligned} \quad (\text{B2})$$

APPENDIX C: NUMERICAL VALIDATION OF THE LOW-TEMPERATURE ASSUMPTION

In Sec. III A we approximate the wave-function overlaps to be close to unity in regimes where $a_0 \ll \lambda_{th}$, see Eq. (19). This assumption was carefully validated by comparing the full numerics we introduced in Ref. [39] to the same numerics with the approximation taken into account. Figure 6 is an exemplary plot for this comparison, showing that in the respective parameter regime the approximation is justified.

APPENDIX D: INTEGRALS OVER WAVE FUNCTIONS

In Sec. III A we introduced abbreviations which essentially give the result of integrals over not only two $\sum_{\mathbf{q}} |\varphi_{\mathbf{q}}|^2 = 1$, but four or six wave functions, to approximate the integrals of Eqs. (B1) and (B2). In 2D this reads

$$\mathcal{F}^{d=2} = \frac{L^2}{a_0^2} \sum_{\mathbf{q}} |\varphi_{\mathbf{q}}|^4 = \frac{4\pi}{5} \quad (\text{D1})$$

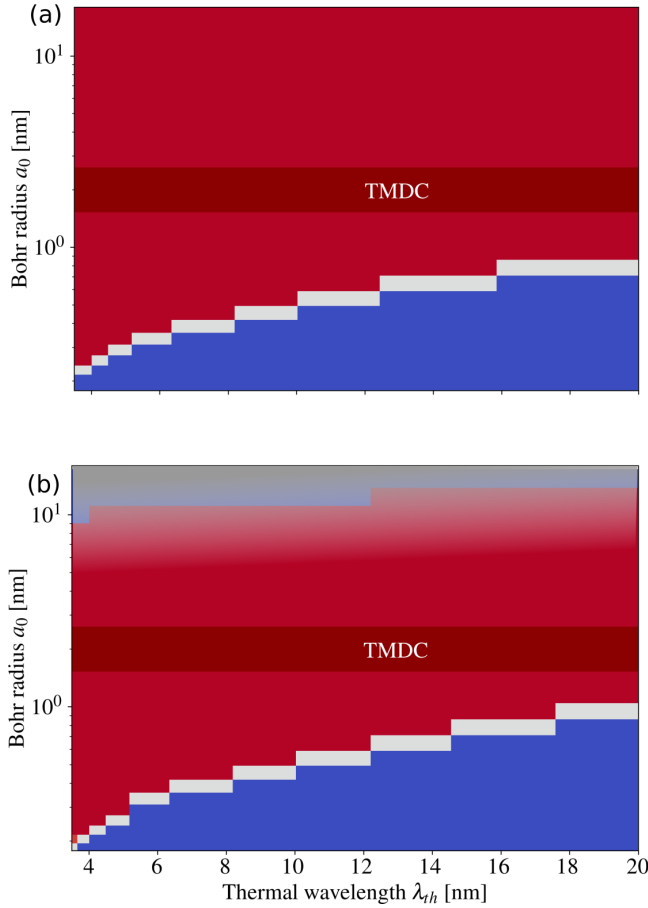


FIG. 6. (a) Full numerics of a 2D realization of Eq. (3) without the low-temperature approximation, similar to the plots Fig. 2 and Fig. S2 in Ref. [39]. (b) Same numerics, with the approximation equation, Eq. (19), applied to all scattering tensors, Eqs. (6), (B1), and (B2). Clearly, the results are very similar for the regime where $\lambda_{th} \gg a_0$ holds.

$$\mathcal{B}^{d=2} = \frac{L^4}{a_0^4} \sum_{\mathbf{q}} |\varphi_{\mathbf{q}}|^6 = \pi^2 \quad (\text{D2})$$

and in 3D,

$$\mathcal{F}^{d=3} = \frac{L^3}{a_0^3} \sum_{\mathbf{q}} |\varphi_{\mathbf{q}}|^4 = \frac{33\pi}{2}, \quad (\text{D3})$$

$$\mathcal{B}^{d=3} = \frac{L^6}{a_0^6} \sum_{\mathbf{q}} |\varphi_{\mathbf{q}}|^6 = \frac{4199\pi^2}{8}. \quad (\text{D4})$$

The computation of the 3D case involves solving integrals with a Schwinger parametrization scheme,

$$\begin{aligned} \int_0^\infty dq q^2 \frac{1}{(1+a_0^2 q^2)^n} &= \frac{1}{\Gamma(n)} \int_0^\infty dq q^2 \int_0^\infty dt t^{n-1} e^{-t(1+a_0^2 q^2)} \\ &= \frac{1}{\Gamma(n)} \int_0^\infty dt t^{n-1} e^{-t} \int_0^\infty dq q^2 e^{-t a_0^2 q^2} \\ &= \frac{\sqrt{\pi}}{4a_0^3 \Gamma(n)} \Gamma\left(n - \frac{3}{2}\right) \end{aligned} \quad (\text{D5})$$

for $n \in \{4, 8, 12\}$, respectively, after applying the analytic expression for the 3D wave function, Eq. (15), and converting

the sum to a three-dimensional integral in spherical coordinates. It can be seen that Eq. (15) fulfills our normalization condition,

$$\sum_{\mathbf{q}} |\varphi_{\mathbf{q}}|^2 = \frac{L^3}{2\pi^2} \int_0^\infty dq q^2 \left| 8\sqrt{\pi a_0^3/L^3} (1+a_0^2 q^2)^{-2} \right|^2 = 1. \quad (\text{D6})$$

The same wave-function model is then again used to evaluate also the higher-order integrals, namely,

$$\begin{aligned} \sum_{\mathbf{q}} |\varphi_{\mathbf{q}}|^4 &= \frac{L^3}{2\pi^2} \int_0^\infty dq q^2 \left| 8\sqrt{\pi a_0^3/L^3} (1+a_0^2 q^2)^{-2} \right|^4 \\ &= \frac{33\pi}{2L^3} a_0^3, \end{aligned} \quad (\text{D7})$$

and

$$\begin{aligned} \sum_{\mathbf{q}} |\varphi_{\mathbf{q}}|^6 &= \frac{L^3}{2\pi^2} \int_0^\infty dq q^2 \left| 8\sqrt{\pi a_0^3/L^3} (1+a_0^2 q^2)^{-2} \right|^6 \\ &= \frac{4199\pi^2}{8L^6} a_0^6. \end{aligned} \quad (\text{D8})$$

From this we can read off the abbreviations as they are given above. The 2D integrals are more straightforward but are treated analogously.

APPENDIX E: THE LIMIT OF SMALL BOHR RADII

Our theory comprises the ideal case of pure bosonic particles for vanishing Bohr radius $a_0 = 0$, where, e.g., in Eqs. (29) and (30) only the nonlinearity for bosonic stimulated scattering prevails, and the bosonic character occurs independent of thermal wavelength (and thus of temperature and particle mass) and independent of the details of the phonon coupling. This limit is shown in Figs. 7(a) and 7(b), respectively. However, this limit is of pure theoretical nature; even for arbitrarily small but finite values of a_0 , the equation remains highly sensitive towards the phonon scattering momentum, as can be seen in the log plot, Figs. 7(c) and 7(d). Even for arbitrarily small Bohr radii the fermionic corrections remain important.

APPENDIX F: EXEMPLARY MATERIAL PARAMETERS FOR MoSe₂

In most of the plots of this work we give exemplary, material realistic values of monolayer MoSe₂ for orientation. The necessary parameters are given in this appendix. In Table I we list standard literature constants in semiconductor units. Table II gives the phonon dispersion of the four phonon modes considered here. Table III gives details on the semiconductor geometry and the dielectric tensor, which is necessary to accurately compute the screening in the material [49,50]. Table IV lists the effective masses of electron and hole, and Table V gives the electron-phonon coupling. All listed values are taken from *ab initio* literature as indicated. For details on the implementation of the parameters and the assumptions concerning the exciton-phonon scattering, see also [39,51,53,67,68].

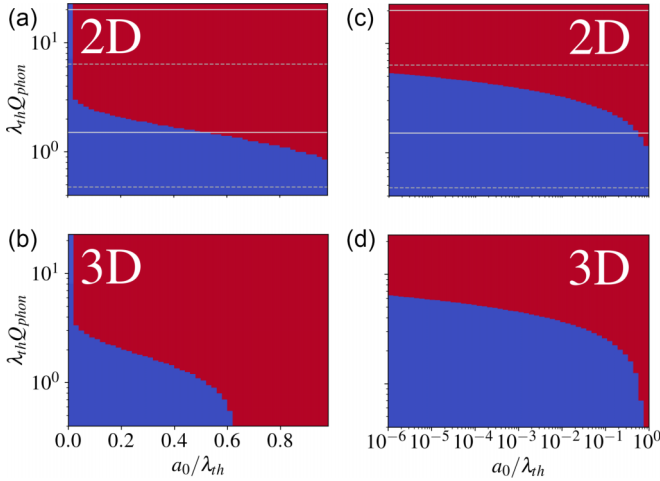


FIG. 7. Plot of the sign of Eqs. (29) and (30). Blue stands for a positive sign of $f(a_0/\lambda_{th}, \lambda_{th}Q_{\text{phon}})$, and red for a negative one, respectively. The gray lines for the 2D plots show temperature-dependent $\lambda_{th}Q_{\text{phon}}$ values for TMDC-like values, i.e., $a_0 = 2$ nm and $M = 1.1 m_{el}$, analogous to Fig. 4. The main point here is that the theoretical limit of $a_0 = 0$ gives ideal bosons that show stimulated scattering independent of the phonon scattering momenta. This limit, however, is not experimentally accessible, as even for arbitrarily small Bohr radii the fermionic corrections remain important.

TABLE I. Important constants in semiconductor units.

e	1 eC
c	299.7925 nm/fs
\hbar	0.658 212 196 eV fs
k_B	$8.617 45 \times 10^{-5}$ eV/K
ϵ_0	$5.526 308 \times 10^{-2}$ eC ² /(eV nm)
μ_0	$2.013 384 742 \times 10^{-4}$ eV fs ² /(eC ² nm)
m_{el}	5.685 680 0 fs ² eV/nm ²
m_p	10 439.604 13 fs ² eV/nm ²

TABLE II. Phonon dispersion. Velocity of sound for the acoustic long-range modes c^i and phonon energies $\hbar\omega^i$ for optical modes, taken from [48].

$c^{LA}/10^{-3}$ nm fs ⁻¹	4.1	$c^{TA}/10^{-3}$ nm fs ⁻¹	4.1
$\hbar\omega^{\Gamma A'}/\text{meV}$	30.3	$\hbar\omega^{\Gamma TO}/\text{meV}$	36.1

TABLE III. General material parameters. We give the lattice constant a_0 and the distance between the two selenium atoms d_0 . Additionally, we require the in-plane component of the respective dielectric tensor.

a_0/nm	0.3319	[77]
d_0/nm	0.343 71	[77]
ϵ_{\perp}	15.27	[69]

TABLE IV. Effective masses taken from first-principle computations (PBE) [45].

m_{eK}^{\uparrow}/m_{el}	0.50
m_{hK}^{\uparrow}/m_{el}	0.60

TABLE V. Electron phonon coupling. Electron phonon coupling parameters in effective deformation potential approximation. The electron phonon matrix element is then given by $g^i = \sqrt{\frac{\hbar}{2\rho\omega^i A}} V_q$, with ρ being the mass density of the unit cell and A being the semiconductor area (which cancels for all calculations). In the case of acoustic long-range phonons, the coupling is given by the first-order deformation potential $V_q = D_1 q$, whereas in the case of optical phonons and zone edge phonons, the coupling is given by zeroth-order deformation potential coupling $V_q = D_0$. The parameters were taken from Refs. [47,48].

Trans. (Momentum)	Conduction band	Valence band		
$K \rightarrow K$ (Γ)	D_1^a/eV	3.4	D_1^a/eV	2.8
	$D_0^e/\text{eV nm}^{-1}$	52	$D_0^e/\text{eV nm}^{-1}$	49

- [1] P. Rivera, J. R. Schaibley, A. M. Jones, J. S. Ross, S. Wu, G. Aivazian, P. Klement, K. Seyler, G. Clark, N. J. Ghimire, J. Yan, D. G. Mandrus, W. Yao, and X. Xu, *Nat. Commun.* **6**, 6242 (2015).
- [2] B. Miller, A. Steinhoff, B. Pano, J. Klein, F. Jahnke, A. Holleitner, and U. Wurstbauer, *Nano Lett.* **17**, 5229 (2017).
- [3] Z. Wang, D. A. Rhodes, K. Watanabe, T. Taniguchi, J. C. Hone, J. Shan, and K. F. Mak, *Nature (London)* **574**, 76 (2019).
- [4] L. Sigl, F. Sigger, F. Kronowetter, J. Kiemle, J. Klein, K. Watanabe, T. Taniguchi, J. J. Finley, U. Wurstbauer, and A. W. Holleitner, *Phys. Rev. Res.* **2**, 042044(R) (2020).
- [5] L. Sigl, M. Troue, M. Katzer, M. Selig, F. Sigger, J. Kiemle, M. Brotons-Gisbert, K. Watanabe, T. Taniguchi, B. D. Gerardot, A. Knorr, U. Wurstbauer, and A. W. Holleitner, *Phys. Rev. B* **105**, 035417 (2022).
- [6] M. Troue, J. Figueiredo, L. Sigl, C. Paspalides, M. Katzer, T. Taniguchi, K. Watanabe, M. Selig, A. Knorr, U. Wurstbauer, and A. W. Holleitner, *Phys. Rev. Lett.* **131**, 036902 (2023).
- [7] F. Lohof, J. Michl, A. Steinhoff, B. Han, M. v. Helversen, S. Tongay, K. Watanabe, T. Taniguchi, S. Höfling, S. Reitzenstein, C. Anton-Solanas, C. Gies, and C. Schneider, *2D Mater.* **10**, 034001 (2023).
- [8] J. M. Blatt, K. W. Böer, and W. Brandt, *Phys. Rev.* **126**, 1691 (1962).
- [9] S. Moskalenko, *Fiz. Tverd. Tela* **4**, 276 (1962) [*Sov. Phys. - Solid State* **4**, 199 (1962)].
- [10] L. Keldysh and Y. V. Kopaev, *Sov. Phys. - Solid State* **6**, 2219 (1965).
- [11] D. Snoke, *Science* **298**, 1368 (2002).
- [12] A. A. High, J. R. Leonard, M. Remeika, L. V. Butov, M. Hanson, and A. C. Gossard, *Nano Lett.* **12**, 2605 (2012).

- [13] M. Alloing, M. Beian, M. Lewenstein, D. Fuster, Y. González, L. González, R. Combescot, M. Combescot, and F. Dubin, *Europhys. Lett.* **107**, 10012 (2014).
- [14] J. Eisenstein, *Annu. Rev. Condens. Matter Phys.* **5**, 159 (2014).
- [15] Y. Morita, K. Yoshioka, and M. Kuwata-Gonokami, *Nat. Commun.* **13**, 5388 (2022).
- [16] O. M. Schmitt, L. Bányai, and H. Haug, *Phys. Rev. B* **60**, 16506 (1999).
- [17] L. Bányai, P. Gartner, O. M. Schmitt, and H. Haug, *Phys. Rev. B* **61**, 8823 (2000).
- [18] O. M. Schmitt, D. B. T. Thoi, L. Bányai, P. Gartner, and H. Haug, *Phys. Rev. Lett.* **86**, 3839 (2001).
- [19] H. Deng, H. Haug, and Y. Yamamoto, *Rev. Mod. Phys.* **82**, 1489 (2010).
- [20] F. Tassone and Y. Yamamoto, *Phys. Rev. B* **59**, 10830 (1999).
- [21] D. Porras, C. Ciuti, J. J. Baumberg, and C. Tejedor, *Phys. Rev. B* **66**, 085304 (2002).
- [22] D. Sarchi and V. Savona, *Phys. Rev. B* **75**, 115326 (2007).
- [23] M. Wouters and I. Carusotto, *Phys. Rev. Lett.* **99**, 140402 (2007).
- [24] X. Ma, Y. V. Kartashov, T. Gao, L. Torner, and S. Schumacher, *Phys. Rev. B* **102**, 045309 (2020).
- [25] C. Lagoin and F. Dubin, *Phys. Rev. B* **103**, L041406 (2021).
- [26] C. Lüders, M. Pukrop, E. Rozas, C. Schneider, S. Höfling, J. Sperling, S. Schumacher, and M. Aßmann, *PRX Quantum* **2**, 030320 (2021).
- [27] F. Cataldini, F. Møller, M. Tajik, J. Sabino, S.-C. Ji, I. Mazets, T. Schweigler, B. Rauer, and J. Schmiedmayer, *Phys. Rev. X* **12**, 041032 (2022).
- [28] B. Remez and N. R. Cooper, *Phys. Rev. Res.* **4**, L022042 (2022).
- [29] C. Lüders, M. Pukrop, F. Barkhausen, E. Rozas, C. Schneider, S. Höfling, J. Sperling, S. Schumacher, and M. Aßmann, *Phys. Rev. Lett.* **130**, 113601 (2023).
- [30] M. Richter, *Phys. Rev. B* **109**, 125308 (2024).
- [31] A. Steinhoff, E. Wietek, M. Florian, T. Schulz, T. Taniguchi, K. Watanabe, S. Zhao, A. Högele, F. Jahnke, and A. Chernikov, *arXiv:2310.18328*.
- [32] L. Pitaevskii and S. Stringari, *Bose-Einstein Condensation and Superfluidity* (Oxford University Press, Oxford, UK, 2016).
- [33] A. L. Ivanov and H. Haug, *Phys. Rev. B* **48**, 1490 (1993).
- [34] A. Steinhoff, M. Florian, M. Rösner, G. Schönhoff, T. O. Wehling, and F. Jahnke, *Nat. Commun.* **8**, 1166 (2017).
- [35] F. Katsch, M. Selig, A. Carmele, and A. Knorr, *Physica Status Solidi B* **255**, 1800185 (2018).
- [36] F. Katsch, M. Selig, and A. Knorr, *Phys. Rev. Lett.* **124**, 257402 (2020).
- [37] F. Katsch and A. Knorr, *Phys. Rev. X* **10**, 041039 (2020).
- [38] C. Trovatiello, F. Katsch, Q. Li, X. Zhu, A. Knorr, G. Cerullo, and S. Dal Conte, *Nano Lett.* **22**, 5322 (2022).
- [39] M. Katzer, M. Selig, L. Sigl, M. Troue, J. Figueiredo, J. Kiemle, F. Sigger, U. Wurstbauer, A. W. Holleitner, and A. Knorr, *Phys. Rev. B* **108**, L121102 (2023).
- [40] A. S. Davydov, *Theory of Molecular Excitons* (Springer US, Boston, MA, 1971).
- [41] F. C. Spano and S. Mukamel, *Phys. Rev. A* **40**, 5783 (1989).
- [42] V. May and O. Kühn, *Charge and Energy Transfer Dynamics in Molecular Systems* (John Wiley & Sons, New York, 2011).
- [43] G. Berghäuser and E. Malic, *Phys. Rev. B* **89**, 125309 (2014).
- [44] H. Haug and S. W. Koch, *Quantum Theory of the Optical and Electronic Properties of Semiconductors*, 5th ed. (World Scientific, Singapore, 2009).
- [45] A. Kormányos, G. Burkard, M. Gmitra, J. Fabian, V. Zólyomi, N. D. Drummond, and V. Fal'ko, *2D Mater.* **2**, 022001 (2015).
- [46] K. Kaasbjerg, K. S. Thygesen, and K. W. Jacobsen, *Phys. Rev. B* **85**, 115317 (2012).
- [47] X. Li, J. T. Mullen, Z. Jin, K. M. Borysenko, M. Buongiorno Nardelli, and K. W. Kim, *Phys. Rev. B* **87**, 115418 (2013).
- [48] Z. Jin, X. Li, J. T. Mullen, and K. W. Kim, *Phys. Rev. B* **90**, 045422 (2014).
- [49] N. S. Rytova, *Moscow Univ. Phys. Bull.* **3**, 18 (1967).
- [50] N. S. Rytova, *arXiv:1806.00976*.
- [51] M. Selig, G. Berghäuser, A. Raja, P. Nagler, C. Schüller, T. F. Heinz, T. Korn, A. Chernikov, E. Malic, and A. Knorr, *Nat. Commun.* **7**, 13279 (2016).
- [52] M. Selig, G. Berghäuser, M. Richter, R. Bratschitsch, A. Knorr, and E. Malic, *2D Mater.* **5**, 035017 (2018).
- [53] M. Selig, F. Katsch, S. Brem, G. F. Mkrtchian, E. Malic, and A. Knorr, *Phys. Rev. Res.* **2**, 023322 (2020).
- [54] J. Sjakste, N. Vast, and V. Tyuterev, *Phys. Rev. Lett.* **99**, 236405 (2007).
- [55] A. Thränhardt, S. Kuckenburg, A. Knorr, T. Meier, and S. W. Koch, *Phys. Rev. B* **62**, 2706 (2000).
- [56] A. Chernikov, V. Bornwasser, M. Koch, S. Chatterjee, C. N. Böttge, T. Feldtmann, M. Kira, S. W. Koch, T. Wassner, S. Lautenschläger, B. K. Meyer, and M. Eickhoff, *Phys. Rev. B* **85**, 035201 (2012).
- [57] D. Feldstein, R. Perea-Causín, S. Wang, M. Dyksik, K. Watanabe, T. Taniguchi, P. Plochocka, and E. Malic, *J. Phys. Chem. Lett.* **11**, 9975 (2020).
- [58] R. Zimmermann, J. Wauer, A. Leitenstorfer, and C. Fürst, *J. Lumin.* **76**, 34 (1998).
- [59] J. Kabuss, S. Werner, A. Hoffmann, P. Hildebrandt, A. Knorr, and M. Richter, *Phys. Rev. B* **81**, 075314 (2010).
- [60] H. Lohmeyer, V. M. Axt, and T. Kuhn, *AIP Conf. Proc.* **772**, 907 (2005).
- [61] G. D. Mahan, in *Polarons in Ionic Crystals and Polar Semiconductors*, edited by J. T. Devreese (North-Holland, Amsterdam, 1972).
- [62] J. T. Devreese and F. Peeters, *Polarons and Excitons in Polar Semiconductors and Ionic Crystals*, Vol. 127 (Springer Science & Business Media, New York, 2013).
- [63] A. Carmele and S. Reitzenstein, *Nanophotonics* **8**, 655 (2019).
- [64] A. Vagov, M. D. Croitoru, V. M. Axt, T. Kuhn, and F. M. Peeters, *Phys. Rev. Lett.* **98**, 227403 (2007).
- [65] H. Haug and A.-P. Jauho, *Quantum Kinetics in Transport and Optics of Semiconductors*, Solid-State Sciences Vol. 123 (Springer, Berlin, Heidelberg, 2008).
- [66] M. Lorke, T. R. Nielsen, J. Seebeck, P. Gartner, and F. Jahnke, *Phys. Rev. B* **73**, 085324 (2006).
- [67] M. Selig, F. Katsch, R. Schmidt, S. Michaelis de Vasconcellos, R. Bratschitsch, E. Malic, and A. Knorr, *Phys. Rev. Res.* **1**, 022007(R) (2019).
- [68] M. Katzer, M. Selig, D. Christiansen, M. V. Ballottin, P. C. M. Christianen, and A. Knorr, *Phys. Rev. Lett.* **131**, 146201 (2023).
- [69] T. C. Berkelbach, M. S. Hybertsen, and D. R. Reichman, *Phys. Rev. B* **88**, 045318 (2013).

- [70] J. Bloch, I. Carusotto, and M. Wouters, *Nat. Rev. Phys.* **4**, 470 (2022).
- [71] H. Haug, *Statistische Physik: Gleichgewichtstheorie* (Springer-Verlag, Berlin, 2006).
- [72] F. Dirnberger, R. Bushati, B. Datta, A. Kumar, A. H. MacDonald, E. Baldini, and V. M. Menon, *Nat. Nanotechnol.* **17**, 1060 (2022).
- [73] D. Christiansen, M. Selig, G. Berghäuser, R. Schmidt, I. Niehues, R. Schneider, A. Arora, S. M. de Vasconcellos, R. Bratschitsch, E. Malic, and A. Knorr, *Phys. Rev. Lett.* **119**, 187402 (2017).
- [74] T. Winzer, A. Knorr, and E. Malic, *Nano Lett.* **10**, 4839 (2010).
- [75] E. Malic, M. Selig, M. Feierabend, S. Brem, D. Christiansen, F. Wendler, A. Knorr, and G. Berghäuser, *Phys. Rev. Mater.* **2**, 014002 (2018).
- [76] V. R. Policht, H. Mittenzwey, O. Dogadov, M. Katzer, A. Villa, Q. Li, B. Kaiser, A. M. Ross, F. Scotognella, X. Zhu, A. Knorr, M. Selig, G. Cerullo, and S. Dal Conte, *Nat. Commun.* **14**, 7273 (2023).
- [77] F. A. Rasmussen and K. S. Thygesen, *J. Phys. Chem. C* **119**, 13169 (2015).